Joint Optimization of Platoon Control and Resource Scheduling in Cooperative Vehicle-Infrastructure System

Peiyu Zhang, Daxin Tian, *Senior Member, IEEE,* Jianshan Zhou, Xuting Duan, Zhengguo Sheng, *Senior Member, IEEE,* Dezong Zhao, *Senior Member, IEEE,* and Dongpu Cao, *Senior Member, IEEE,*

***Abstract*—Vehicle platooning technology is essential in achieving group consensus, on-road safety, and fuel-saving. Meanwhile, Vehicle-to-Infrastructure (V2I) communication significantly facilitates the development of connected vehicles. However, the coupled effects of the longitudinal vehicle's mobility, platoon control and V2I communication may result in a low reliable communication network between the platoon vehicle and the roadside unit, there is a tradeoff between the platoon control and communication reliability. In this paper, we investigate a bi-objective joint optimization problem where the first objective is to maximize the success probability of data transmission (communication reliability) and the second objective function is to minimize the traffic oscillation flow. The vehicle's mobility state of the platoon vehicle affects the channel capacity and transmission performance. In this context, we deeply explore the relationship between control signals and resource scheduling and theoretically deduce a closed-form expression of the optimal communication reliability objective. Through this closed expression, we transform the bi-objective model into a single objective MPC model by using ϵ-constraint method. We design an efficient algorithm for solving the joint optimization model and prove the convergence. To verify the effectiveness of the proposed method, we finally evaluate the spacing error, speed error, and resource scheduling of platooning vehicles through simulation experiments in two experimental scenarios. The results show that the proposed control-communication co-design can improve the platoon control performance while satisfying the high reliability of V2I communications.**

***Index Terms*—Cooperative vehicle-infrastructure systems (CVIS), vehicle platooning, Vehicle-to-Infrastructure (V2I) communication, multi-objective optimization**

This research was supported in part by the National Key Research and Development Program of China under Grant No. 2022YFC3803700, in part by the National Natural Science Foundation of China under Grant No. U20A20155, Grant No. 52202391, Grant No. 62061130221 and Grant No. 62173012. *(Corresponding author: Daxin Tian.)*

Peiyu Zhang, Daxin Tian, Jianshan Zhou, Xuting Duan are with the Beijing Key Laboratory for Cooperative Vehicle Infrastructure Systems and Safety Control, Beijing Advanced Innovation Center for Big Data and Brain Computing, School of Transportation Science and Engineering, Beihang University, Beijing 100191, China (e-mail: zpeiyu2@163.com; jianshanzhou@foxmail.com; dtian@buaa.edu.cn; duanxuting@buaa.edu.cn).

Zhengguo Sheng is with the Department of Engineering and Design, University of Sussex, Richmond, Brighton BN1 9RH, U.K. (e-mail: z.sheng@sussex.ac.uk).

Dezong Zhao is with the James Watt School of Engineering, University of Glasgow, Glasgow G12 8QQ, U.K. (e-mail: dezong.zhao@glasgow.ac.uk).

Dongpu Cao is with the Department of Mechanical and Mechatronics Engineering, University of Waterloo, Waterloo, ON N2L 3G1, Canada (e-mail: dongpu.cao@uwaterloo.ca).

I. Introduction

Advanced 5G, vehicular communication, platoon control techniques, etc., have promoted the development of Cooperative Vehicle Infrastructure Systems (CVIS) [1]. By adopting effective management methodologies, CVIS can provide a safe, coordinated traffic network that improves traffic capacity and smoothness and enhances road safety [2]. A connected vehicle platoon is an advanced technology in which a group of vehicles operates together while constantly coordinating the inter-vehicle speed. Self-organization of networked vehicles into a platoon improves the road capacity and prevents traffic congestion [3]–[5]. Moreover , the vehicles in a platoon can provide passengers with a comfortable experience, especially on long trips [6].

Autonomous vehicle formation requires two advanced communication technologies: Vehicle-to-Vehicle (V2V) and Vehicle-to-Infrastructure (V2I). V2V communication allows sharing of the speed and position information between the vehicles connected in the platoon and other surrounding vehicles [7], and V2I communication ensures the interaction of information between the vehicles/platoons and the infrastructure, providing valuable predictive information to the platooning vehicles [8], [9]. For example, the infrastructure processes the data collected from the platoon and other data sources and makes it accessible to other devices, facilitating coordination between regional vehicles. In addition, the upper-layer applications associated with cooperative control of the platooning vehicles need high-performance communication for data transmission. This communication helps the cloud to enable environmental perception and drive decisions [10]. In general, a platoon-based cooperative vehicle infrastructure system requires a joint optimization strategy for both platoon control and data transfer.

Nevertheless, data transmission by V2I communication in vehicular platoon mobility environments faces several challenges. On the one hand, the design of control systems and vehicle communication systems is based on different and often competing principles. For example, frequent information sampling can improve the platooning control performance in a high vehicle mobility environment but requires an extensive communication bandwidth [11]. Meanwhile, sending large amounts of real-time data over the channel may lead to network congestion and consequent channel contention, increased latency, and packet loss, which negatively affect the

control performance [12]. Therefore, stable and reliable data transfer between vehicles and the infrastructure is not easily achieved during vehicle platooning. On the other hand, vehicle platoon systems require relatively complex engineering. The control objective of the platoon is to satisfy transient and asymptotic dynamics, including vehicle mobility, safe distance, and stability. However, the problem of optimizing data transmission reliability has received little attention in the vehicle platoon control literature [13]. In addition, the conventional V2I communication networks focus only on the mobility and security of individual vehicles, which conflicts with the optimal performance of the platoon. Thus, the V2I communication typologies may be inapplicable to platooning vehicles in a high-mobility environment. Moreover, many of the existing optimization problems of control and communication solve a single objective [14], [15]. To satisfy the vehicular application demands of service quality, two coupled objectives, i.e., the control objectives and communication reliability objectives, must be solved simultaneously to achieve vehicular mobility, platooning control, and communication.

In this paper, we present a bi-objective joint optimization model that couples vehicle platoon control with vehicular communication. Specifically, we consider vehicular mobility, platooning control, and V2I-communication reliability in different models. Based on the vehicle mobility, V2I channel characteristics and platoon control, we characterize the V2I communication reliability of the platooning vehicles and present a new bi-objective joint optimization model. Specifically, the first objective is maximizing communication reliability and the second objective is to minimize traffic oscillation (platoon safety). In particular, we theoretically characterize the V2I communication reliability, including stochastic V2I channel fading, time-varying formation vehicle location and resource scheduling schemes. We also derive a closed-form expression for the reliability-optimal transmission scheduling solution and the optimal reliability thus establishing a theoretical link between channel conditions, platooning vehicles' mobility and data transmission. These theoretical derivations promote the novel design of our joint optimization solution. Finally, using this expression and leveraging the ϵ-constraint method, we transform the original non-convex bi-objective model into a computationally tractable model. The main contributions of our work are summarized below.

- We propose a novel bi-objective joint optimization model for predictive platooning control and reliability-oriented communication in vehicle-infrastructure systems. The objective of the model is to stabilize the platooning vehicles while guaranteeing the reliability of V2I communications. The model jointly optimizes the control inputs of the platooning vehicles and schedules their data transmissions to the infrastructure at the same time.
- We theoretically characterize the V2I communication reliability from a probabilistic perspective. Considering the characteristics of the V2I channel and the mobility of the platooning vehicles. We also analytically derive an expression for optimal communication reliability. Using this expression and leveraging the ϵ-constraint method, we transform the original non-convex bi-objective model into a computationally tractable model.
- We theoretically prove that our joint optimization method always converges. We conduct extensive simulations in different platooning scenarios and verify the superior V2I communication reliability and control stability of our joint optimization model.

The remainder of this paper is organized as follows. Section II overviews related work and Section III develops the system model for a controlled platoon-based vehicular communication network, including the bi-objective joint optimization model for a platoon and a goal programming based on the ϵ-constraint method. An algorithm for the joint optimization problem is designed in Section IV and utilized in a simulation study in Section V. Conclusions and future research directions are presented in Section VI.

II. Related Work

Cooperative control of connected and autonomous platooning vehicles has recently attracted substantial attention in control engineering. Platooning has been realized by different control methods [16]. For example, [17] employed a data-driven method to describe the high-dimensional state of platoon vehicles, then proposed a distributed predictive control method that keeps the spacing between vehicles in mixed vehicle platoons. The control objective is to coordinate the movement of vehicles on the road at a constant speed. [18] presented a distributed MPC model for vehicle platoon control problems with communication delay. [19] proposed a Pareto optimal information flow topology to improve the control performance and fuel consumption indexes. In addition, [20] designed a CACC controller by combining linear quadratic regulator (LQR) and parameter space approach for the distributed cooperative vehicular platoon. To achieve platoon control in dense traffic scenarios, [21] proposed a predictive control scheme that satisfies the smaller communication requirements of the platoon vehicles while being robust to communication disturbances. However, it is not only concerning the platoon controller design in the cooperative vehicle-infrastructure system but also the reliable communication between the platoon and infrastructure that is worthy of attention.

Joint optimization problems of control and communication are gaining traction and some researchers are developing innovative design solutions for resource scheduling to the infrastructure in a vehicle platoon mobility environment. Different systems models and optimization goals for joint design can be found in the literature [22]–[24]. Based on the coupled characteristics of air-to-ground communications, [22] developed a two-dimensional control scheme for platooning vehicles and optimized the weighted global energy efficiency of an air-to-ground communication system. [23] proposed a control-communication co-design for reliable platooning. Specifically, they developed a two-timescale reinforcement learning framework to minimize the inter-vehicle distance while satisfying the V2I quality-of-service. [24] analysed the impact between communications and motion control of CAV and proposed a communication-control joint optimization

algorithm for CAV control. Although several optimization methods have been developed to address the joint design of vehicle trajectories, communication and computation, few studies have provided insights into reliability-oriented platooning control, particularly a theoretical description of the reliability of data transmission between platooning vehicles and the infrastructure from a probabilistic perspective.

Moreover, models that optimize platoon control multi-objectives have also been published. For example, [25] designed a centralized MPC controller for a platoon at signalized segregated intersections. This controller has three goals: platoon safety, fuel consumption, and intersection throughput. The multi-objective model was solved using the weighted-sum method. [26] proposed an eco-driving optimization model for mixed platooning vehicles under vehicle safety, fuel economy, and operating time objectives. They designed the algorithms and optimized the vehicle trajectory based on a two-stage optimization ideology. [27] developed a non-dominated sorting genetic algorithm that obtains a set of Pareto solutions for optimizing the driving comfort performance under multiple objectives. [28] proposed a multi-objective H_∞ control strategy for distributed vehicle platoon system to reduce the inter-vehicle distances, while the stability of the system can be ensured

However, in the vehicle infrastructure system, it is not enough to only consider the control performance of the platooning vehicles, it is also necessary to consider the reliability of data transmission between the platoon vehicles and the infrastructure through the V2I channel. This is because vehicle mobility, queuing control objectives and reliability of V2I communication are mutually coupled. Currently, vehicle communication security issues have been tackled in models that jointly consider individual vehicle communication and mobility control. Considering vehicle mobility, channel contention, and channel fading, [29] evaluated the reliability of data transmission over V2I links and developed a stochastic model of the probability of successful data transmission. Taking a different approach, [30] developed a cluster-based communication framework that optimizes the quality of service of a given controller among vehicular nodes. The communication network aims to minimize the cost of exclusive-use channels. Related problems were addressed by [31]–[33]. Although these works contribute essential research value, they are insufficient because they separately consider vehicle platoon control and communication optimization. Works that fully consider communication resource scheduling for platoon control are very scarce. Moreover, most of the studies on communication protocols provide no insights into beacon-performance compliance with the platoon control requirements [30]. The interaction between platoon control and vehicular communication in vehicle infrastructure cooperative systems requires further investigation. First, the coupled effects of vehicle mobility, channel contention, and communication resource scheduling should be incorporated into the overall design. Second, two performance indicators (platoon control and communication) should be included in the optimization formulation.

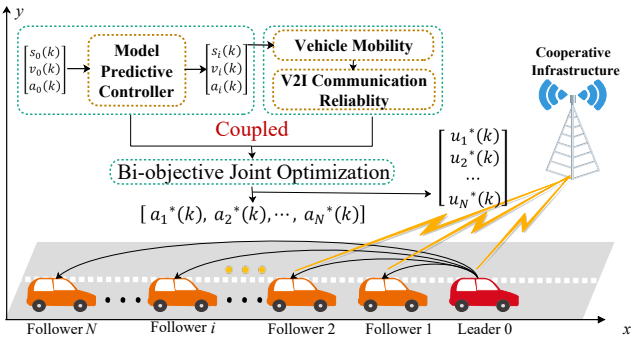

Fig. 1: The implementation framework of the proposed joint optimization method.

III. System Model and Problem Formulation

Fig. 1 shows the platoon-based vehicular communication network scenario of the present study. The vehicles in a platoon can offload application-layer data to the infrastructure via V2I communication. A longitudinal control design improves traffic efficiency and guarantees the safety of the platooning vehicles. However, the mobility of vehicles in the platooning process will dynamically affect the relative geographical distance between the vehicles and infrastructure, and hence the data transmission performance of the communication link. Therefore, the mobility in the platooning process and communication of the vehicles are inherently coupled. For this purpose, we develop a framework that jointly optimizes platooning and V2I communications.

A. Coupling Analysis of Vehicle Mobility, Platoon Control and V2I Communication

1) Vehicular Mobility Formulation: In this scenario, N + 1 vehicles drive along a straight road. Vehicle 0 is the leader and vehicles 1 to N are followers. All moving vehicles are equipped with sensors enabling information sharing of real-time traffic status, such as position, speed and control signals. The finite control horizon is discredited into K time slots, each of duration τ seconds. Let $\mathcal{K} = \{1, \cdots K\}$ represent the set of time slot indexes and $\mathcal{N} = \{1, \cdots N\}$ represent the set of platooning vehicle indexes. The longitudinal dynamics of vehicle i in each time interval $[k\tau,\ (k+1)\tau)$ for $k \in \mathcal{K}$ is then described by the following discrete-time linear model

$$\begin{cases} s_i(k+1) = s(k) + \tau v_i(k) + \frac{\tau^2}{2} a_i(k),\ i \in \mathcal{N}; \\ v_i(k+1) = v_i(k) + \tau a_i(k),\ i \in \mathcal{N}, \end{cases} \tag{1}$$

where $s_i(k)$ and $v_i(k)$ represent the longitudinal position and speed of vehicle i, respectively, at time step k, and $a_i(k)$ represents the acceleration/deceleration (i.e., control variable) of vehicle i at control sample point k.

During the platooning process, the mobility of vehicles will dynamically affect the relative geographical distance between the vehicles and their infrastructure and ultimately affects the V2I communication performance of data transmission. There also exists a ground infrastructure (e.g., a central cloud) that receives and processes the data volume from the moving

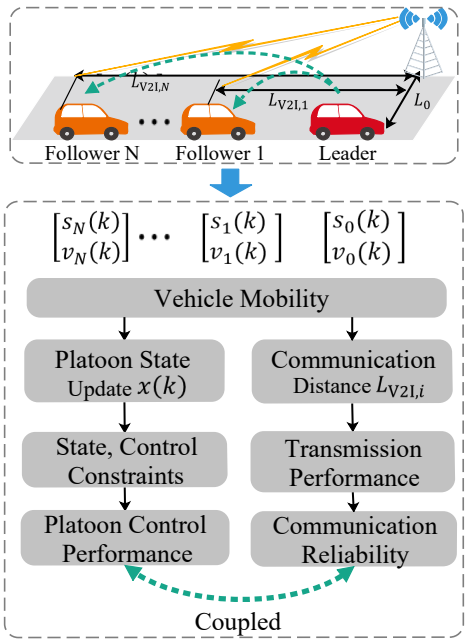

Fig. 2: Coupling analysis.

vehicles. As shown in Fig. 2, $L_{\text{V2I},i}$ denotes the initial distance between platooning vehicle i and the infrastructure and L_0 is the relative vertical distance between the infrastructure and the roadway. Thus the time-varying relative distance $L_i(a_i(k))$ between the infrastructure and vehicle i is calculated as

$$L_i(a_i(k)) = \sqrt{\left[L_{\text{V2I},i} - s_i(k)\right]^2 + L_0^2}, \quad i \in \mathcal{N}, \tag{2}$$

where the initial distance $L_i(a_i(k))$ is related to the control vector $a_i(k)$, and $s_i(k)$ is denoted by model (1).

2) Coupling Analysis: The joint optimization problem simultaneously considers platoon control and V2I communication. The MPC controller allows speed tracking of the leading vehicle by all followers. The relative distance between two vehicles should converge to the desired distance d_i. During the platoon formation, the control signal $a_i(k)$ will dynamically affect the mobile trajectory and further affect the relative distance $L_i(a_i(k))$ between the vehicle and the infrastructure, ultimately affecting the probability of successful data transmission. The mobility of the platooning vehicles also affects the performance of data transmission.

B. Modeling of V2I Communication Reliability

1) V2I Channel Model: Applying the Shannon theorem [34], the channel capacity C_i between the infrastructure and vehicle i in the platoon is formulated as

$$C_i(a_i(k)) = \frac{B}{M} \log_2 \left[1 + w_i \cdot g^2(L_i(a_i(k)))\right], \ k \in \mathcal{K}, \tag{3}$$

where B is the available bandwidth, and M is the number of vehicles accessing the infrastructure at the same time under the constraint $M \geq N$. The normalized power w_i is related to the noise-to-signal ratio $\frac{S}{\varpi}$, where S is the V2I transmission power and ϖ is the average noise strength. $g(L_i(a_i(k)))$ is the distance-dependent cellular V2I channel gain.

2) V2I Transmission Performance: Supposing that the V2I communication of each pair link through Rayleigh fading channel [35], which makes $g(L_i(a_i(k)))$ obey an exponential distribution with the parameter $L_i(a_i(k))$. The variable $u_i(k)$ defines the amount of data transmitted from vehicle i to the infrastructure within time slot k. The success probability of data transmission from platooning vehicle i to the cooperative infrastructure is then given by

$$\begin{aligned} p_i\left(u_i(k), a_i(k)\right) &= \text{Prob}\left\{C_i(a_i(k)) \geq \frac{u_i(k)}{\tau}\right\} \\ &= \exp\left(-\frac{2^{\frac{u_i(k)M}{B\tau}} - 1}{w_i} L_i^2(a_i(k))\right). \end{aligned} \tag{4}$$

For each platooning vehicle i, let $\theta_{\text{out},i}$ be the total application-layer data to be sent. Partitioning the data content into a sequence of smaller pieces, i.e., $\theta_{\text{out},i} = \sum_{k=1}^{K} u_i(k)$, we can optimize a series of smaller files $\{u_i(k) \geq 0, i \in \mathcal{N}, k \in \mathcal{K}\}$ and thus estimate the data transmission of vehicle i during the whole time slot K. By the multiplication principle, the overall success probability of data transmissions over all time slots is

$$\begin{aligned} P_i\left(\boldsymbol{u}_i, a_i(k)\right) &= \prod_{k=1}^{K} p_i\left(u_i(k), a_i(k)\right) \\ &= \exp\left(-\frac{\sum_{k=1}^{K} L_i^2(a_i(k)) 2^{\frac{u_i(k)M}{B\tau}}}{w_i} + \frac{\sum_{k=1}^{K} L_i^2(a_i(k))}{w_i}\right), \end{aligned} \tag{5}$$

where the vector $\boldsymbol{u}_i = [u_i(1), \ldots, u_i(K)]$.

Using (5), we now characterize the overall V2I communication reliability of the whole platooning vehicles as follows

$$\begin{aligned} H(\boldsymbol{u}, a_i(k)) &= \sum_{i=1}^{N} P_i\left(u_i(k), a_i(k)\right) \\ &= \sum_{i=1}^{N} \exp\left(\frac{\sum_{k=1}^{K} L_i^2(a_i(k))}{w_i} - \frac{\sum_{k=1}^{K} L_i^2(a_i(k)) 2^{\frac{u_i(k)M}{B\tau}}}{w_i}\right), \end{aligned} \tag{6}$$

where the decision vector of data transmission $\boldsymbol{u} = \{\boldsymbol{u}_1, \ldots, \boldsymbol{u}_N\}$. As shown in the above equation, the communication reliability $H(\boldsymbol{u}; \boldsymbol{a})$ is closely related to the vehicle mobility in the platoon.

C. Modeling of Platooning Control

From a control perspective, we aim to stabilize the vehicle platoon by minimizing the inter-vehicle tracking errors. A centralized MPC controller of the following vehicles enables speed tracking of the lead vehicle and ensures a constant travel distance d_i. To simplify the illustration, the distance and speed between vehicle $i-1$ and i are defined as

$$\begin{cases} g_i^v(k) = v_{i-1}(k) - v_i(k); \\ g_i^s(k) = s_{i-1}(k) - s_i(k). \end{cases} \tag{7}$$

Based on the discrete-time linear model (1), the following constraints and objectives are imposed on the control framework.

1) Constraints of Platoon Control:

- All the following vehicles satisfy the acceleration constraints, i.e.,

$$a_{\min} \leq a_i(k) \leq a_{\max},\ i \in \mathcal{N}, k \in \mathcal{K}, \tag{8}$$

where $a_{\max}$ and $a_{\min}$ are the maximal and minimal accelerations, respectively.

- The speed error $g_i^v(k)$ between vehicles $i-1$ and i must satisfy the given platoon performance requirement, i.e.,

$$e_{\min}^v \leq g_i^v(k) \leq e_{\max}^v,\ i \in \mathcal{N}, k \in \mathcal{K}, \tag{9}$$

where $e_{\min}^v \leq 0$ and $e_{\max}^v \geq 0$ are the minimal and maximal allowable speed errors between vehicles $i-1$ and i, respectively. Constraints (9) improve the speed performance of the platoon by reducing the traffic flow oscillations of speed changes.

- The distance error between vehicles $i-1$ and i satisfies the following safety distance requirement:

$$e_{\min}^s \leq g_i^s(k) - d_i \leq e_{\max}^s,\ i \in \mathcal{N}, k \in \mathcal{K}. \tag{10}$$

Constraints (10) improve the spacing error of the platoon by ensuring that the distance between two vehicles is asymptotically stable and finally becomes constant d_i. In these constraints, $e_{\min}^s$ and $e_{\max}^s$ are the minimal and maximal distance errors between vehicles $i-1$ and i, respectively. The distance error $g_i^v(k)$ can take any value within the bounds $[d_i + e_{\min}^s, d_i + e_{\max}^s]$.

Hence, the state spaces between vehicles $i-1$ and i are defined as $\triangle s_i(k+1) = g_i^s(k) - d_i$ and $\triangle v_i(k+1) = g_i^v(k)$. Based on model (1), the platooning system of vehicle i is

$$\begin{aligned}\begin{bmatrix}\triangle s_i(k+1)\\ \triangle v_i(k+1)\end{bmatrix} = \begin{bmatrix}1 & \tau\\ 0 & 1\end{bmatrix}\begin{bmatrix}\triangle s_i(k)\\ \triangle v_i(k)\end{bmatrix} + \begin{bmatrix}\frac{\tau^2}{2}\\ \tau\end{bmatrix} a_{i-1}(k)\\ + \begin{bmatrix}-(\frac{\tau^2}{2})\\ -\tau\end{bmatrix} a_i(k).\end{aligned} \tag{11}$$

Assume that $\boldsymbol{x}_i(k+1) = [\triangle s_i(k+1), \triangle v_i(k+1)]^\top$, (11) can be converted to

$$\boldsymbol{x}_i(k+1) = \mathbf{A}\boldsymbol{x}_i(k) + \mathbf{B}a_{i-1}(k) + \mathbf{D}a_i(k), \tag{12}$$

where $\mathbf{A} = \begin{bmatrix}1 & \tau\\ 0 & 1\end{bmatrix}$, $\mathbf{B} = \begin{bmatrix}\frac{\tau^2}{2}\\ \tau\end{bmatrix}$, $\mathbf{D} = \begin{bmatrix}-(\frac{\tau^2}{2})\\ -\tau\end{bmatrix}$.

$$\begin{aligned}\boldsymbol{x}(k) &= \mathrm{col}\{\boldsymbol{x}_1(k), \boldsymbol{x}_2(k), \ldots, \boldsymbol{x}_N(k)\},\\ \boldsymbol{a}(k) &= \mathrm{col}\{a_1(k), a_2(k), \ldots, a_N(k)\}.\end{aligned} \tag{13}$$

Furthermore, the state of the total platoon system can be compactly represented as

$$\boldsymbol{x}(k+1) = \boldsymbol{G}_A\boldsymbol{x}(k) + \boldsymbol{G}_B\boldsymbol{a}(k) + \boldsymbol{G}_D a_0(k) \tag{14}$$

where the system matrices $\boldsymbol{G}_A$ and $\boldsymbol{G}_B$ are defined by

$$\begin{aligned}\boldsymbol{G}_A &= \mathrm{diag}\{\boldsymbol{A}, \boldsymbol{A}, \ldots, \boldsymbol{A}\} \in \mathbb{R}^{2N\times 2N}\\ \boldsymbol{G}_D &= \mathrm{col}\{\boldsymbol{D}, \mathbf{0}, \mathbf{0}, \cdots, \mathbf{0}\} \in \mathbb{R}^{2N\times 1}\end{aligned}$$

$$\boldsymbol{G}_B = \begin{bmatrix}\boldsymbol{D} & \mathbf{0} & \mathbf{0} & \cdots & \mathbf{0} & \mathbf{0}\\ \boldsymbol{B} & \boldsymbol{D} & \mathbf{0} & \cdots & \mathbf{0} & \mathbf{0}\\ \mathbf{0} & \boldsymbol{B} & \boldsymbol{D} & \cdots & \mathbf{0} & \mathbf{0}\\ \vdots & \vdots & \vdots & \ldots & \vdots & \vdots\\ \mathbf{0} & \mathbf{0} & \mathbf{0} & \cdots & \boldsymbol{B} & \boldsymbol{D}\end{bmatrix}$$

In our platoon system, the state $\boldsymbol{x}_0(k)$ and control $a_0(k)$ of leading vehicle can be designed in advance. At an equilibrium state, the speed of leading vehicle is v_0, therefore, we can set $a_0(k) = 0$ within this equilibrium. Based on the constraints (9), (10) and (11), we define

$$\begin{aligned}\boldsymbol{a}_{\min} &= \mathrm{col}\{a_{\min},\ i \in \mathcal{N}\};\\ \boldsymbol{a}_{\max} &= \mathrm{col}\{a_{\max},\ i \in \mathcal{N}\};\\ \boldsymbol{x}_{\min} &= \mathrm{col}\{e_{\min}^s, e_{\min}^v,\ i \in \mathcal{N}\};\\ \boldsymbol{x}_{\max} &= \mathrm{col}\{e_{\max}^s, e_{\max}^v,\ i \in \mathcal{N}\},\end{aligned} \tag{15}$$

then the set of state constraints and control constraints for all platooning vehicles are

$$\begin{cases}\boldsymbol{x}_{\min} \leq \boldsymbol{x}(k) \leq \boldsymbol{x}_{\max}, k \in \mathcal{K}; & (16)\\ \boldsymbol{a}_{\min} \leq \boldsymbol{a}(k) \leq \boldsymbol{a}_{\max}, k \in \mathcal{K}. & (17)\end{cases}$$

In order to deduce a more compact form over the prediction horizon K, we further drive

$$\boldsymbol{X} = \boldsymbol{M}_A\boldsymbol{x}(k|k) + \boldsymbol{M}_B\boldsymbol{a} \tag{18}$$

where

$$\begin{cases}\boldsymbol{X} = \mathrm{col}\{\boldsymbol{x}(1), \boldsymbol{x}(2), \ldots, \boldsymbol{x}(K)\},\\ \boldsymbol{a} = \mathrm{col}\{\boldsymbol{a}(1), \boldsymbol{a}(2), \ldots, \boldsymbol{a}(K)\}.\end{cases} \tag{19}$$

Moreover, $\boldsymbol{M}_A$, $\boldsymbol{M}_B$ and $\boldsymbol{C}$ are defined by

$$\boldsymbol{M}_A = \mathrm{col}\left\{\boldsymbol{G}_A^1, \boldsymbol{G}_A^2, \ldots, \boldsymbol{G}_A^K\right\} \in \mathbb{R}^{2NK\times 2N}$$

$$\boldsymbol{M}_B = \begin{bmatrix}\boldsymbol{G}_B & \mathbf{0} & \mathbf{0} & \cdots & \mathbf{0}\\ \boldsymbol{G}_A\boldsymbol{G}_B & \boldsymbol{G}_B & \mathbf{0} & \cdots & \mathbf{0}\\ \boldsymbol{G}_A^2\boldsymbol{G}_B & \boldsymbol{G}_A\boldsymbol{G}_B & \boldsymbol{G}_B & \cdots & \mathbf{0}\\ \vdots & \vdots & \vdots & \cdots & \vdots\\ \boldsymbol{G}_A^{K-1}\boldsymbol{G}_B & \boldsymbol{G}_A^{K-2}\boldsymbol{G}_B & \boldsymbol{G}_A^{K-3}\boldsymbol{G}_B & \cdots & \boldsymbol{G}_B\end{bmatrix}$$

In addition, the set of state constraints (16) and control constraints (17) of all vehicles are

$$\begin{cases}\boldsymbol{X}_{\min} \leq \boldsymbol{X} \leq \boldsymbol{X}_{\max}; & (20)\\ \widetilde{\boldsymbol{a}}_{\min} \leq \boldsymbol{a} \leq \widetilde{\boldsymbol{a}}_{\max}. & (21)\end{cases}$$

where

$$\begin{aligned}&\widetilde{\boldsymbol{a}}_{\min} = \mathrm{col}\{\boldsymbol{a}_{\min},\ k \in \mathcal{K}\}; \widetilde{\boldsymbol{a}}_{\max} = \mathrm{col}\{\boldsymbol{a}_{\max},\ k \in \mathcal{K}\};\\ &\boldsymbol{X}_{\min} = \mathrm{col}\{\boldsymbol{x}_{\min},\ k \in \mathcal{K}\}; \boldsymbol{X}_{\max} = \mathrm{col}\{\boldsymbol{x}_{\max},\ k \in \mathcal{K}\},\end{aligned} \tag{22}$$

2) Objective of Platoon Control: The objective of the vehicular platoon is to reduce the change rates of spacing and speed of all followers. The followers can track the speed of the leader while maintaining the desired distance d_i. Hence, the cost function of the MPC design of the platoon over the prediction horizon $k, k \in \mathcal{K}$ takes the following quadratic form,

$$J(\boldsymbol{X}, \boldsymbol{a}) = \left[\boldsymbol{X}^\top\mathbf{Q}\boldsymbol{X} + \boldsymbol{a}\mathbf{R}\boldsymbol{a}\right] \tag{23}$$

where $\mathbf{Q}$ and $\mathbf{R}$ are symmetric and positive definite matrices. The objective of the platoon control is to minimize the oscillations of the platoon under the prediction horizon K. The first item reduces the state error between two adjacent vehicles and the second item controls the magnitude of the control input $\boldsymbol{a}$.

D. Bi-objective Joint Optimization Model

To achieve vehicle platoon control and data transmission in the operative vehicle infrastructure system, we simultaneously optimize two objectives: maximizing the success probability of data transmissions (6) and minimizing the oscillation (23) of the platoon. Based on the above analysis, we develop a bi-objective joint optimization model for the platoon-based vehicular communication network. The joint optimization model combines the vehicle mobility, platoon control, and communication reliability-related model and is formulated as follows

$$
\begin{aligned}
M_1: &\max_{\boldsymbol{u},\ \boldsymbol{a}}: H(\boldsymbol{u},\boldsymbol{a}) \\
&\min_{\boldsymbol{a}}: J(\boldsymbol{X},\boldsymbol{a}) \\
&\text{s.t.} \begin{cases} \boldsymbol{X}=\boldsymbol{M}_A\boldsymbol{x}(k|k)+\boldsymbol{M}_B\boldsymbol{a}; \\ \boldsymbol{X}_{\min}\le \boldsymbol{X}\le \boldsymbol{X}_{\max}; \\ \widetilde{\boldsymbol{a}}_{\min}\le \boldsymbol{a}\le \widetilde{\boldsymbol{a}}_{\max}; \\ \boldsymbol{x}(k+K|k)=\boldsymbol{0}; \\ u_i(k)\ge 0,\ i\in\mathcal{N},k\in\mathcal{K}; \\ \sum_{k=1}^{K} u_i(k)=\theta_{\text{out},i},\ i\in\mathcal{N}. \end{cases}
\end{aligned} \tag{24}
$$

Model (24) includes two coupled objectives of the vehicle platoon: communication reliability and platoon safety. Based on the function $H(\boldsymbol{u},\boldsymbol{a})$, we develop a reliability-oriented optimal V2I data scheduling scheme $u_i^*(k)\ge 0, i\in\mathcal{N},k\in\mathcal{K}$ for the platoon, which maximizes the probability of successful data transmission. Through the cost function $J(\boldsymbol{x},\boldsymbol{a})$, we develop a series of optimal control inputs $a_i^*(k), i\in\mathcal{N},k\in\mathcal{K}$ of the platoon to minimize the tracking error. In addition, to ensure the stability of the platoon, the terminal equality constraint $\boldsymbol{x}(k+K|k)=\boldsymbol{0}$ is added to the platoon control problem. According to [36], these terminal equality constraints can guarantee the closed-loop stability and the system stability analysis is shown by Theorem 2 in the next section.

Clearly, M_1 is a complex dynamic optimization model that combines the two objectives of platoon control and V2I communication under a set of constraints. In general, this model is non-convex and is very difficult to solve directly. Thus, in the following sections, we will describe our novel optimization method for solving the bi-objective model.

IV. Model Analysis

In this Section, we leverage the ϵ-constraint method [37] to convert the bi-objective joint optimization model M_1 to a single objective model. Next, we provide the closed-loop stability analysis of the proposed joint optimization model.

A. Objective analysis

Obviously, the platooning control objective conflicts with the communication reliability objective, preventing the simultaneous optimization of both objectives. Therefore, we solve the two objectives model using the ϵ-constraint method. The optimization design of the ϵ-constraint method involves two main steps.

Step 1: Based on the mobility of platooning vehicles and the V2I communication resource scheduling design scheme and applying first-order optimality theory, we theoretically derive the maximum objective $H_{\max}(\boldsymbol{u}^*,\boldsymbol{a})$ as the following sub-model:

$$
\begin{aligned}
&\max_{\boldsymbol{u}}:\ H(\boldsymbol{u},\boldsymbol{a}) \\
&\text{s.t.} \begin{cases} \sum_{k=1}^{K} u_i(k)=\theta_{\text{out},i}\ i\in\mathcal{N}; \\ u_i(k)\ge 0,\ i\in\mathcal{N},k\in\mathcal{K}. \end{cases}
\end{aligned} \tag{25}
$$

where $u_i(k), i\in\mathcal{N},k\in\mathcal{K}$ is a data transmission solution of V2I communication, and $a_i(k), i\in\mathcal{N},k\in\mathcal{K}$ denotes a control solution of the platoon. To facilitate the solution process, we equivalently convert sub-model (25) to the following form

$$
\begin{aligned}
&\min_{\boldsymbol{u}}:\ \sum_{i=1}^{N}\sum_{k=1}^{K} L_i^2(a_i(k))[2^{\frac{u_i(k)M}{B\tau}}-1] \\
&\text{s.t.} \begin{cases} \sum_{k=1}^{K} u_i(k)=\theta_{\text{out},i}\ i\in\mathcal{N}; \\ u_i(k)\ge 0,\ i\in\mathcal{N},k\in\mathcal{K}. \end{cases}
\end{aligned} \tag{26}
$$

To derive the maximum objective $H_{\max}(\boldsymbol{u}^*,\boldsymbol{a})$ and obtain the closed-form optimal data transmission volume $u_i^*(k), i\in\mathcal{N},k\in\mathcal{K}$, we provide the following Lemma and Theorem based on sub-model (26). To facilitate the presentation, we derive

$$
F(\boldsymbol{u},\boldsymbol{a})=\sum_{i=1}^{N}\sum_{k=1}^{K} L_i^2(a_i(k))[2^{\frac{u_i(k)M}{B\tau}}-1]. \tag{27}
$$

Lemma 1: Suppose that $\boldsymbol{u}_i^*=\{u_i^*(1),u_i^*(2),\ldots,u_i^*(K)\}^\top$ is the optimal data transmission volume from vehicle i to the infrastructure in model (26). For two non-zero optimal solutions $u_i^*(\ell_1)>0, u_i^*(\ell_1)\in\boldsymbol{u}_i^*$ and $u_i^*(\ell_2)>0, u_i^*(\ell_1)\in\boldsymbol{u}_i^*$ with $\ell_1\ne\ell_2$, the following equations hold

$$
\frac{\partial F(u_i(k),a_i(k))}{\partial u_i^*(\ell_1)}=\frac{\partial F(u_i(k),a_i(k))}{\partial u_i^*(\ell_2)}.
$$

In contrast, the zero optimal solution $u_i^*(\ell_3)=0, u_i^*(\ell_3)\in\boldsymbol{u}_i^*$ with $\ell_1\ne\ell_2\ne\ell_3$ satisfies the following inequality

$$
\begin{aligned}
\frac{\partial F(u_i(k),a_i(k))}{\partial u_i^*(\ell_3)}&\ge\frac{\partial F(u_i(k),a_i(k))}{\partial u_i^*(\ell_1)}, \\
\frac{\partial F(u_i(k),a_i(k))}{\partial u_i^*(\ell_3)}&\ge\frac{\partial F(u_i(k),a_i(k))}{\partial u_i^*(\ell_2)}.
\end{aligned}
$$

Proof: Please refer to Appendix A. ■

Combining *Lemma 1*, we further derive the maximum value of the objective $H_{\max}(\boldsymbol{u}^*,\boldsymbol{a})$ and obtain the relationship between optimal solution $u_i^*(k), i\in\mathcal{N},k\in\mathcal{K}$ and control signs $a_i(k), i\in\mathcal{N},k\in\mathcal{K}$ of model (26) in *Theorem 1*.

Theorem 1: When the data transmission volume $\{u_i^*(k)\ge 0, i\in\mathcal{N},k\in\mathcal{K}\}$ of platooning vehicle i is optimized in model (25), the following expression always holds:

$$
u_i^*(k)=\frac{B\tau\left[\sum_{k=1}^{K}\log_2 L_i^2(a_i(k))-\log_2 L_i^2(a_i(k))\right]}{MK}+\frac{\theta_{\text{out},i}}{K}, \tag{28}
$$

for $i \in \mathcal{N}, k \in \mathcal{K}$ and $u_i^*(k) \geq 0$. Accordingly, the optimal objective $H_{\max}(\boldsymbol{u}^*; \boldsymbol{a})$ takes the form

$$H_{\max}(\boldsymbol{u}^*, \boldsymbol{a}) = \sum_{i=1}^{N} \exp\left(\frac{\sum_{k=1}^{K} L_i^2(a_i(k))}{w_i}\right) \times \exp\left(-\frac{K \cdot 2^{\frac{\theta_{\text{out},i} M}{K B \tau}} \left(\prod_{k=1}^{K} L_i^2(\mathbf{a}_i(k))\right)^{\frac{1}{K}}}{w_i}\right). \tag{29}$$

Proof: The optimal solutions $u_i^*(k) > 0, i \in \mathcal{N}, k \in \mathcal{K}$ satisfy

$$\begin{aligned} &\frac{\partial F(u_i^*(k), a_i(k))}{\partial u_i^*(k)} = \lambda_i \\ \Rightarrow &\frac{\partial \left(\sum_{i=1}^{N} \sum_{k=1}^{K} L_i^2(a_i(k))[2^{\frac{u_i(k) M}{B\tau}} - 1]\right)}{\partial u_i^*(k)} = \lambda_i. \end{aligned} \tag{30}$$

Assuming $r = \frac{M}{B\tau}$, we further obtain

$$L_i^2(a_i(k)) \cdot 2^{u_i^*(k) r} \cdot r \ln 2 = \lambda_i. \tag{31}$$

From (31), we deduce

$$u_i^*(k) = \frac{\log_2(\lambda_i) - \log_2\left(L_i^2(a_i(k))\right) - \log_2(r \ln 2)}{r}. \tag{32}$$

For platooning vehicle i in all time slots K, we have

$$\sum_{k=1}^{K} L_i^2(a_i(k)) \cdot 2^{u_i^*(k) r} = \frac{K \lambda_i}{r \ln 2}. \tag{33}$$

Inserting Eq. (33) into (6) and rearranging, the success probability of data transmission of this platoon is

$$H_{\max}(\boldsymbol{u}^*, \boldsymbol{a}) = \sum_{i=1}^{N} \exp\left(\frac{K \lambda_i}{r y_i \ln 2} + \frac{\sum_{k=1}^{K} L_i^2(a_i(k))}{y_i}\right). \tag{34}$$

Multiplying the optimal solutions within each time slot in (33), we then obtain

$$(\lambda_i)^K = \left(\prod_{k=1}^{K} L_i^2(a_i(k)\right) 2^{r \sum_{k=1}^{K} u_i^*(k)} (r \ln 2)^K. \tag{35}$$

As $\sum_{k=1}^{K} u_i^*(k) = \theta_{\text{out},i}, i \in \mathcal{N}$, we get

$$\lambda_i = \left(\prod_{k=1}^{K} L_i^2(a_i(k)\right)^{\frac{1}{K}} 2^{\frac{r \theta_{\text{out},i}}{K}} (r \ln 2). \tag{36}$$

Substituting (36) into (32) and (34), the proof is realized immediately. ■

Step 2, to obtain the maximum upper bound $H_{\max}(\boldsymbol{u}^*, \boldsymbol{a})$ of model (25), we transform the communication reliability objective (6) into a constraint bounded by $(1-\epsilon)H_{\max}(\boldsymbol{u}^*, \boldsymbol{a})$ where ϵ is the objective reduction rate. Finally, the bi-objective joint optimization model is converted into a single objective model M_2

$$M_2 \quad : \min_{\boldsymbol{u}, \boldsymbol{a}} : J(\boldsymbol{u}, \boldsymbol{a})$$
$$\text{s.t.} \begin{cases} H(\boldsymbol{u}, \boldsymbol{a}) \geq (1-\epsilon) H_{\max}(\boldsymbol{u}^*, \boldsymbol{a}); \\ \boldsymbol{X} = \boldsymbol{M}_A \boldsymbol{x}(k|k) + \boldsymbol{M}_B \boldsymbol{a}; \\ \boldsymbol{X}_{\min} \leq \boldsymbol{X} \leq \boldsymbol{X}_{\max}; \\ \widetilde{\boldsymbol{a}}_{\min} \leq \boldsymbol{a} \leq \widetilde{\boldsymbol{a}}_{\max}; \\ \boldsymbol{x}(k+K|k) = \boldsymbol{0}; \\ u_i(k) \geq 0, \ i \in \mathcal{N}, k \in \mathcal{K}; \\ \sum_{k=1}^{K} u_i(k) = \theta_{\text{out},i}, \ i \in \mathcal{N}. \end{cases} \tag{37}$$

where $\epsilon \in [0, 1]$ is the decrease rate of the maximum of the communication reliability objective $H_{\max}(\boldsymbol{u}^*, \boldsymbol{a})$, which is solved by the model (25). This method removes the difficulties of solving the bi-objective model. Fig. 3 shows the implementation framework of the proposed objective optimization. In the next section, we propose an iterative algorithm for solving model M_2 and prove its convergence to a local optimum.

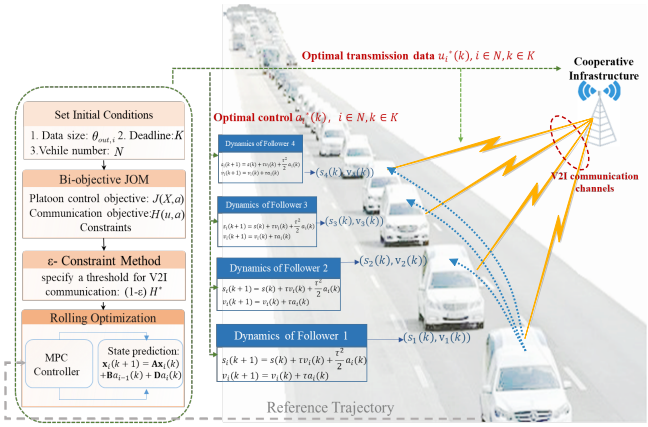

Fig. 3: The implementation framework of the proposed method .

B. System Stability Analysis

In this section, we provide the stability analysis of the platooning vehicles in our joint optimization model M_2. The main strategy is to create a reasonable Lyapunov function for the platoon system and prove that it is decreasing. we adopt the local cost function as a Lyapunov function and provide the following Theorem to discuss the closed-loop stability of the MPC low (14).

Theorem 2: Suppose that $\mathbf{Q}$ and $\mathbf{R}$ are symmetric and positive definite matrices, Then, for all initial states, $\boldsymbol{x}(k|k)$ satisfy $\boldsymbol{x}_{\min} \leq \boldsymbol{x}(k|k) \leq \boldsymbol{x}_{\max}$, the receding horizon control strategy $\boldsymbol{a}$ obtained by the optimization problem (24) minimizing the cost function $J(\boldsymbol{u}, \boldsymbol{a})$ to make the platoon system asymptotically stable.

Proof: Please refer to Appendix B. ■

Based on the assumptions of Theorem 2, the optimal objective is monotonically decreasing and consequently, the control system of the platoon is asymptotically stable.

V. Proposed optimization algorithm

This section presents the algorithm for solving the joint optimization model M_2. First, we integrate the constraints into the original model and simplify it to model M_3. Applying the theory of successive convex approximation, we transform the extended model into a series of convex optimization sub-models and solve them using a sequential quadratic programming iterative algorithm. The optimal solution of the original model is then obtained.

A. Iterative Optimization Algorithm

For simplicity, we reorganize the equation and inequality constraints in model (37) into $C_m(\mathbf{U}) = 0$ and $C_z(\mathbf{U}) \geq 0$, respectively, where $m \in \mathcal{M}$ and $z \in \mathcal{Z}$. The total numbers of indices $\mathcal{M}$ and $\mathcal{Z}$ are $2NK + N$ and $5NK + 1$, respectively. The expressions of $C_m(\mathbf{U})$ and $C_z(\mathbf{U})$ are detailed in Appendix C. Now, letting $\mathbf{U} = [a_i(k), u_i(k), i \in \mathcal{N}, k \in \mathcal{K}]^\top$, (37) is transformed into the equivalent form M_3

$$M_3 : \min_{\mathbf{U}} : J(\mathbf{U}) \quad \text{s.t.} \begin{cases} C_m(\mathbf{U}) = 0, m \in \mathcal{M}; \\ C_z(\mathbf{U}) \geq 0, z \in \mathcal{Z}. \end{cases} \tag{38}$$

The optimization model (38) at iteration point $t + 1$ is updated as follows

$$\mathbf{U}_{t+1} = \mathbf{U}_t + \boldsymbol{\alpha}_t \mathbf{d}_t, \tag{39}$$

where $\mathbf{d}_t$ is the direction of descent in neighborhood $\mathbf{U}_t$ and $\boldsymbol{\alpha}_t$ is the step size in this direction. The update formula requires a suitable range of feasible descent directions and step sizes.

To solve this nonlinear optimization problem, we employ the sequential quadratic programming (SQP) method (38), which approximates the Hessian matrix of the Lagrangian function at each iteration using a Newtonian approach. Using this matrix, it then generates a quadratic programming subproblem whose solution is the search direction $\mathbf{d}_t$ of the search process [38], [39].

The Lagrangian function of the optimization problem (38) is defined as

$$L(\mathbf{U}, \boldsymbol{\lambda}) = J(\mathbf{U}) - \sum_{m \in \mathcal{M}} \lambda_m C_m(\mathbf{U}) - \sum_{z \in \mathcal{Z}} \lambda_z C_z(\mathbf{U}), \tag{40}$$

$\boldsymbol{\lambda} = \{\lambda_r,\ r \in \mathcal{M} \cup \mathcal{Z}\}^\top$. After linearizing the nonlinear constraint, the quadratic optimization sub-model is expressed as follows:

$$\text{S-}M_3 : \min_{\mathbf{d}} : \nabla_{\mathbf{U}} J(\mathbf{U}_t)^\top \mathbf{d} + 0.5 \mathbf{d}^\top \mathbf{O}_t \mathbf{d} \quad \text{s.t.} \begin{cases} C_m(\mathbf{U}_t) + \nabla_{\mathbf{U}} C_m(\mathbf{U}_t)^\top \mathbf{d}_t = 0, m \in \mathcal{M}; \\ C_z(\mathbf{U}_t) + \nabla_{\mathbf{U}} C_n(\mathbf{U}_t)^\top \mathbf{d}_t \geq 0, n \in \mathcal{Z}, \end{cases} \tag{41}$$

where $\mathbf{O}_t$ is the Hessian matrix defined in the quasi-Newton approximation of the Lagrangian function. From this expression, we derive the search direction $\mathbf{d}$. Applying the Broyden–Fletcher–Goldfarb–Shanno method, the update formula of $\mathbf{O}_t$ is obtained as

$$\mathbf{O}_{t+1} = \mathbf{O}_t - \frac{\mathbf{O}_t \mathbf{R}_t \mathbf{R}_t^\top \mathbf{O}_t}{\mathbf{R}_t^\top \mathbf{B}_t \mathbf{R}_t} + \frac{\mathbf{s}_t \mathbf{s}_t^\top}{\mathbf{s}_t^\top \mathbf{R}_t}, \tag{42}$$

where $\mathbf{R}_t = \mathbf{U}_{t+1} - \mathbf{U}_t$ denotes the displacement and $\mathbf{s}_t$ denotes the gradient difference between steps t and $t + 1$.

$$\mathbf{s}_t = \nabla_{\mathbf{U}} L(\mathbf{U}_{t+1}, \boldsymbol{\lambda}_t) - \nabla_{\mathbf{U}} L(\mathbf{U}_t, \boldsymbol{\lambda}_t). \tag{43}$$

The Hessian matrix $\mathbf{O}_{t+1}$ generated from the update equation (42) is guaranteed positive definite when the matrix $\mathbf{O}_{t+1}$ is symmetric positive definite.

The convex quadratic programming sub-model is solved to obtain a feasible search direction $\mathbf{d}_t$ for the new $\mathbf{U}_{t+1}$. Next, we construct a suitable step size $\boldsymbol{\alpha}_t$ such that the objective of model (38) decreases along the search direction $\mathbf{d}_t$ at each iteration t. The iterations must converge to a feasible region in model (38). Following the literature [31], we determine the value of $\boldsymbol{\alpha}_t$ using the exact penalty function method. The penalty function is defined as

$$G(\mathbf{U}, \boldsymbol{\pi}) = J(\mathbf{U}) + \sum_{m \in \mathcal{M}} \pi_m |C_m(\mathbf{U})| + \sum_{z \in \mathcal{Z}} \pi_z [\max(0, C_z(\mathbf{U}))], \tag{44}$$

where $\boldsymbol{\pi} = \{\pi_r, r \in \mathcal{M} \cup \mathcal{Z}\}^\top$ are the penalty coefficients. Combining the Lagrange multipliers $\boldsymbol{\lambda}$, we update the penalty coefficients $\boldsymbol{\pi}$ using Powell's update formula [40]. The updating process is

$$\pi_{r,t} = \begin{cases} |\lambda_{r,t}|, t = 1 \\ \max\left\{|\lambda_{r,t}|, \frac{1}{2}(|\lambda_{r,t}| + \pi_{r,t-1})\right\}, t \geq 2 \end{cases} \tag{45}$$

for $r \in \mathcal{M} \cup \mathcal{Z}$. In (45), $\pi_{r,t}$ and $\lambda_{r,t}$ represent the penalty parameters and Lagrangian coefficients at iteration t, respectively. In the updating process of $\boldsymbol{\pi}$, the penalty function $G(\mathbf{U}, \boldsymbol{\pi})$ always decreases. Based on (44) and (45), we present the following search model with step size $\boldsymbol{\alpha}_t$ at iteration t

$$\boldsymbol{\alpha}_t \in \min_{\boldsymbol{\alpha} \in \mathbb{R}_+} \{G(\mathbf{U}_t + \boldsymbol{\alpha} \mathbf{d}_t, \boldsymbol{\pi}_t)\}.$$

B. Convergence Analysis

We now describe the SQP-based method that implements the non-convex model (37). The overall optimization framework is shown in algorithm 1. Later, we will discuss the convergence of the proposed algorithm.

Lemma 2: Let $(\mathbf{U}_t,\ \boldsymbol{\lambda}_t)$ be a point sequence satisfying the KKT condition and let $\boldsymbol{\pi}_t$ be a penalty factor satisfying (45). For $\mathbf{d}_t$ obtained by model (41), the penalty function $G(\mathbf{U}_t, \boldsymbol{\pi}_t, \boldsymbol{d}_t)$ is monotonically decreasing.

Proof: Please refer to Appendix D ■

Based on the above results and the following *Theorem 2*, we here analyze the convergence of algorithm 1.

Theorem 3: Suppose that $\pi_{r,t} \geq |\lambda_{r,t}|$, $r \in \mathcal{M} \cup \mathcal{Z}$ for each $t \geq 1$, and $(\mathbf{U}_t, \mathbf{d}_t)$ is the point sequence of tth sub-model generated by Algorithm 1. Assuming that $\lim_{t \to \infty} \mathbf{d}_t = 0$, then the point sequence$\{\mathbf{U}_t, t \geq 1\}$ is converge to the KKT points of the original model (6).

Algorithm 1: The algorithm design for the joint optimization model M_2

Input: Permissible velocity $0 \leq \sigma \ll 1$, maximum number of iterations T;
Initialization: Iterative number $t = 1$;
Rearrange original model M_2 to M_3;
for $t \leq T$ **do**
  Initialize $\mathbf{U}_1[t]$, $\mathbf{O}_1[t]$ and set $j = 1$;
  Transform model M_3 to a quadratic programming model S-M_3;
  repeat
    Get $\mathbf{d}_j[t]$ by solving sub-model S-M_3;
    Determine a proper step size $\boldsymbol{\alpha}_j$ in the direction $\mathbf{d}_j[t]$;
    Update $\mathbf{U}_{j+1}[t] = \mathbf{U}_j[t] + \boldsymbol{\alpha}_j \mathbf{d}_j[t]$;
    if $\|\nabla_{\mathbf{U}} L(\mathbf{U}_{j+1}[t], \lambda)\| > \sigma$ **then**
      Revise $\mathbf{O}_{j+1}[t]$ by using BFGS method;
      Update $j = j + 1$;
  until $\|\nabla_{\mathbf{U}} L(\mathbf{U}_{j+1}[t], \lambda)\| \leq \sigma$;
  Update $\mathbf{U}^*[t] = \mathbf{U}_{j+1}[t]$;
  Update $t = t + 1$
Output: The optimal solution $\mathbf{U}^*$ and the optimal objective $J(\mathbf{U}^*)$

Proof: According to the positive characteristic of $\mathbf{O}_t$ and the boundedness of the Lagrangian multipliers $\boldsymbol{\lambda}_t$, we can deduce the following equations hold

$$\lim_{t\to\infty} \mathbf{O}_t = \mathbf{O}^*, \lim_{t\to\infty} \boldsymbol{\lambda}_t = \boldsymbol{\lambda}^*, \lim_{t\to\infty} \mathbf{U}_t = \mathbf{U}^*.$$

Obviously, $(\mathbf{d}^*, \boldsymbol{\lambda}^*)$ is a KKT pair of sub-model (41) where $\lim_{t\to\infty} \mathbf{d}_t = \mathbf{d}^*$. The KKT conditions of the model (41) are given as

$$\begin{cases} \lambda^*_{z,t} \geq 0; \\ C_z(\mathbf{U}^*) + \nabla_{\mathbf{U}} C_z(\mathbf{U}^*)^{\mathrm{T}} \mathbf{d}^* \geq 0; \\ \lambda^*_{z,t} \left(C_z(\mathbf{U}^*) + \nabla_{\mathbf{U}} C_z(\mathbf{U}^*)^{\mathrm{T}} \mathbf{d}^* \right) = 0; \\ C_m(\mathbf{U}^*) + \nabla_{\mathbf{U}} C_m(\mathbf{U}^*)^{\mathrm{T}} \mathbf{d}^* = 0; \\ \nabla_{\mathbf{U}} J(\mathbf{U}^*) + \mathbf{O}^* \mathbf{d}^* - \sum_{r\in\mathcal{M}\cup\mathcal{Z}} \lambda^*_{r,d} \nabla_{\mathbf{U}} C_r(\mathbf{U}^*) = 0. \end{cases} \tag{46}$$

Based on the above discussion, we only need to prove $\mathbf{d}^* = \mathbf{0}$ that the theorem can be finished. Next, we perform the following contradictory proof.

Assuming that $\mathbf{d}^* \neq \mathbf{0}$, we have

$$\lim_{t\to\infty} \mathbf{U}_t + \hat{\boldsymbol{\alpha}} \mathbf{d}_t = \mathbf{U}^* + \hat{\boldsymbol{\alpha}} \mathbf{d}^*, \tag{47}$$

where $\hat{\boldsymbol{\alpha}} = \min_{\boldsymbol{\alpha}\in\mathbb{R}_+} \{G(\mathbf{U}^* + \boldsymbol{\alpha}\mathbf{d}^*, \boldsymbol{\pi})\}$. According to *lemma 2*, the penalty function is monotonically decreasing and we can obtain

$$\varphi = G(\mathbf{U}^*, \boldsymbol{\pi}) - G(\mathbf{U}^* + \hat{\boldsymbol{\alpha}}\mathbf{d}^*, \boldsymbol{\pi}) > 0. \tag{48}$$

Combining (47) and (48), we deduce

$$\begin{aligned} &\lim_{t\to\infty} \{G(\mathbf{U}_t + \hat{\boldsymbol{\alpha}}\mathbf{d}_t, \boldsymbol{\pi}) + \varphi/2\} \\ =&\lim_{t\to\infty} \{G(\mathbf{U}_t + \hat{\boldsymbol{\alpha}}\mathbf{d}_t, \boldsymbol{\pi}) - G(\mathbf{U}^* + \hat{\boldsymbol{\alpha}}\mathbf{d}^*\boldsymbol{\pi})\}/2 \\ &+ \lim_{t\to\infty} \{G(\mathbf{U}_t + \hat{\boldsymbol{\alpha}}\mathbf{d}_t, \boldsymbol{\pi}) + G(\mathbf{U}^*, \boldsymbol{\pi})\}/2 \\ =&[G(\mathbf{U}^*, \boldsymbol{\pi}) + G(\mathbf{U}^* + \hat{\boldsymbol{\alpha}}\mathbf{d}^*, \boldsymbol{\pi})]/2 < G(\mathbf{U}^*, \boldsymbol{\pi}). \end{aligned} \tag{49}$$

At each iteration $t \geq 1$, we have

$$G(\mathbf{U}_{t+1}, \boldsymbol{\pi}) \leq G(\mathbf{U}_t, \boldsymbol{\pi}) + \varepsilon_k, \tag{50}$$

and

$$\frac{\varphi}{2} > \sum_{p=k}^{\infty} \varepsilon_k. \tag{51}$$

At a sufficiently large iteration $t \in \mathbb{N}_+$, we have

$$\begin{aligned} &\lim_{t\to\infty} G(\mathbf{U}_{t+2}, \boldsymbol{\pi}) \leq \lim_{t\to\infty} \{G(\mathbf{U}_{t+1}, \boldsymbol{\pi})\} + \sum_{p=t+1}^{\infty} \varepsilon_p \\ \Rightarrow &G(\mathbf{U}^*, \boldsymbol{\pi}) \leq \lim_{t\to\infty} \{G(\mathbf{U}_t + \hat{\boldsymbol{\alpha}}\mathbf{d}_t, \boldsymbol{\pi})\} + \sum_{p=t+1}^{\infty} \varepsilon_p \\ \Rightarrow &G(\mathbf{U}^*, \boldsymbol{\pi}) < \{G(\mathbf{U}^* + \hat{\boldsymbol{\alpha}}\mathbf{d}^*, \boldsymbol{\pi})\} + \varphi/2 < G(\mathbf{U}^*, \boldsymbol{\pi}). \end{aligned} \tag{52}$$

As the above formula is contradictory, we have $\lim_{t\to\infty} \mathbf{d}_t = \mathbf{d}^* = \mathbf{0}$. Inserting this result into the KKT condition (46), the optimal solution $\mathbf{U}^*$ becomes the KKT points of the original model (37). The theorem is thus proven. ■

VI. Simulation Experiment

This Section evaluates the proposed bi-objective joint optimization model in simulations. We first describe our simulation settings and then show the results of the proposed joint optimization model. Then, we conduct comparison experiments to observe the V2I communication reliability and platoon control. All simulation experiments were implemented in Matbal/Simulink-based solver version R2020 running on a 2.8-GHz 64-bit Core i7-8400U CPU machine under Windows 10 Professional.

A. Simulation Settings

In the application scenarios (see Fig. 1), a platoon is formed from one leading vehicle and four followers. The vehicles aim to coordinate their space headway and stabilize their velocities while transmitting their application-layer data to a roadside infrastructure.

TABLE I: Parameters settings in model

Parameter	Value	Parameter	Value
N	4	M	150
K	35 s	τ	0.5 s
ϵ	3×10^{-5}	d_i	10 m
$a_{\min}$	$-2.5\,\mathrm{m/s^2}$	$a_{\max}$	$+2.5\,\mathrm{m/s^2}$
$e^v_{\min}$	$-6\,\mathrm{m/s}$	$e^v_{\max}$	$+6\,\mathrm{m/s}$
$e^s_{\min}$	$-3\,\mathrm{m}$	$e^s_{\max}$	$+3\,\mathrm{m}$
$D_{\mathrm{out},i}$	5×10^6 bits	B	10 Mbit
ϖ	$-96\,\mathrm{dBm}$	S	1 W
L_0	50 m	$L_{\mathrm{V2I},0}$	200 m

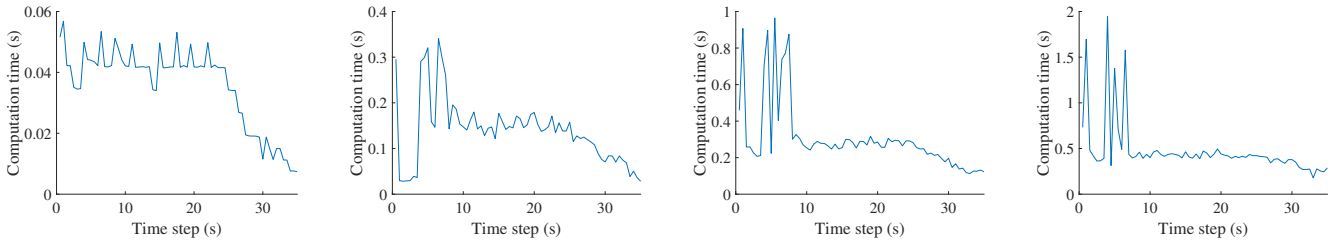

(a) $N_p = 2\,\mathrm{s}$ (b) $N_p = 3\,\mathrm{s}$ (c) $N_p = 4\,\mathrm{s}$ (d) $N_p = 5\,\mathrm{s}$

Fig. 4: Computation performance under different N_p in Scenario 1.

Based on literature [18], we properly adopt vehicle mobility parameters. Besides, we also set the parameters for the V2I communication by referring to literature [29]. Specifically, the initial state of the lead vehicle is: $s_0(0) = 0\,\mathrm{m}$ and $v_0(0) = 10\,\mathrm{m/s}$. Besides, the initial space distance between the vehicles in the platoon is $10\,\mathrm{m}$ and the initial speed of the four following vehicles is $10\,\mathrm{m/s}$. Table I summarizes the other parameter settings in the platooning mobility of vehicles and physical-layer communication. In addition, two different experimental scenarios are considered to validate the performance of the proposed method.

- **Scenario 1:** The leading vehicle momentarily accelerates/decelerates for a fixed period before maintaining a constant speed. This design scenario tests whether data transmission can be guaranteed while maintaining a stable speed and distance when the vehicle in front suddenly accelerates or decelerates. In both scenarios, the acceleration/deceleration of the platooning was collected every $0.5\,\mathrm{s}$ and the sample time is designed as $\tau = 0.5\,\mathrm{s}$. The acceleration and deceleration of the leading vehicle are listed below

$$a_0(k) = \begin{cases} 0.5\,\mathrm{m/s^2} & k \in [3.5, 5.5]\,\mathrm{s} \\ 1\,\mathrm{m/s^2} & k \in [6, 7.5]\,\mathrm{s} \\ 0.5\,\mathrm{m/s^2} & k \in [8, 10]\,\mathrm{s} \\ -0.5\,\mathrm{m/s^2} & k \in [14.5, 16.5]\,\mathrm{s} \\ -1\,\mathrm{m/s^2} & k \in [17, 18.5]\,\mathrm{s} \\ -1\,\mathrm{m/s^2} & k \in [19, 21]\,\mathrm{s} \\ 0\,\mathrm{m/s^2} & \text{others} \end{cases}$$

- **Scenario 2:**The leading vehicle will accelerate or decelerate periodically. This scenario aims to test whether the proposed joint optimization scheme can reduce the periodic speed and interval fluctuation and ensure the success of data transmission. In this scenario, the acceleration/deceleration of the leading vehicle changes periodically with $\pm 1\,\mathrm{m/s^2}$ from $k = 8\,\mathrm{s}$ to $k = 20\,\mathrm{s}$. In addition, since the sampling time τ is $0.5\,\mathrm{s}$, the change period is $2\,\mathrm{s}$, then the vehicle maintains its original speed after $k = 25\,\mathrm{s}$.

In both experimental scenarios, the motion states of the leading vehicle were varied to observe whether the four following vehicles could simultaneously achieve trajectory tracking and resource scheduling with the cooperative infrastructure.

B. Selection of Prediction and Control Horizon Parameters

The performance of the joint optimization model is affected by the control horizon N_c and the prediction horizon N_p. On the one hand, the predictive horizon should be large enough so that the model can accurately predict the control step of more time slots. When the predictive time horizon increases, the MPC controller of the platoon can predict longer distances, and its performance will improve accordingly. On the other hand, if the prediction horizon is excessively long, model mismatch and disturbance of the MPC controller may occur, increasing the calculation time of the optimization and the difficulty of implementing the control input online. The same tradeoff applies when selecting the control horizon. To minimize the above problems, we conducted a tuning analysis of the MPC parameters for different predictive horizons ($N_p = 2\,\mathrm{s}$, $N_p = 3\,\mathrm{s}$, $N_p = 4\,\mathrm{s}$, $N_p = 5\,\mathrm{s}$). The control horizon was $N_c = 0.5\,\mathrm{s}$. Fig. 4 compares the computational performances of algorithm 1 in the different N_p cases of Scenario 1. The means and variances of the computational times in each step are presented in Table II. The computational time increased with increasing prediction horizon N_p and surpassed the control horizon $N_c = 0.5\,\mathrm{s}$ at $N_p > 5$. Therefore, $N_p > 5$ yielded a low control performance, and the joint optimization algorithm could not operate in real time. In all following case studies, the parameters of the control and prediction horizons were set to $N_c = 0.5\,\mathrm{s}$ and $N_p = 4\,\mathrm{s}$, respectively.

TABLE II: The mean and variance of computation time

Prediction horizon	Computation times (s)	
	Mean	Variance
$N_p = 2\,\mathrm{s}$	0.0358	1.72E-06
$N_p = 3\,\mathrm{s}$	0.1381	0.0051
$N_p = 4\,\mathrm{s}$	0.2981	0.0326
$N_p = 5\,\mathrm{s}$	0.4738	0.0942

C. Convergence Validation

Fig.7 compares the evolutions of the descent-function value for different partial time slots k. The objective function of the joint optimization model decreased within an appropriate number of iterations and converged to a locally optimal point, confirming that the proposed joint optimization method can reach a steady state. The average number of iterations among all time slots is 24, indicating that a local solution can be found within a finite number of iterations. Therefore, the numerical performance of the proposed joint optimization algorithm is deemed satisfactory for real-time computation.

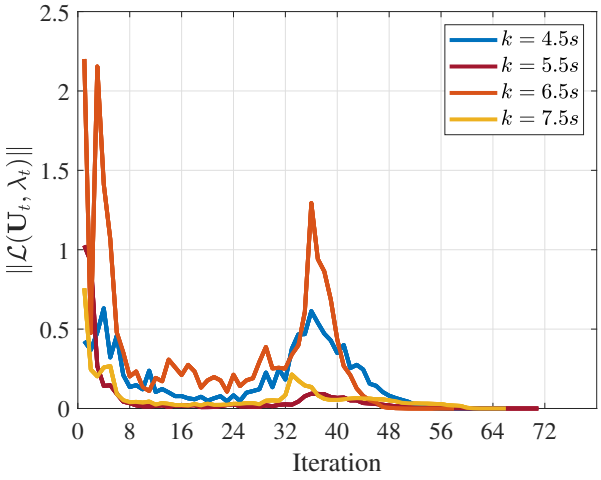

Fig. 7: The convergence of the Algorithm in Scenario 1.

D. Experimental Results

The results of the joint optimization model in **Scenario 1** are depicted in Fig. 5. Fig. 5(a) shows the vehicle accelerations(i.e., control inputs) $\{a_i(k), i \in \mathcal{N}, k \in \mathcal{K}\}$, speeds $\{v_i(k), i \in \mathcal{N}, k \in \mathcal{K}\}$ and longitudinal positions $\{s_i(k), i \in \mathcal{N}, k \in \mathcal{K}\}$ of the platoon vehicles. It can be shown that the accelerations of the vehicle are in the range of [-2.5 $\mathrm{m/s^2}$, 2.5 $\mathrm{m/s^2}$], each follower is able to track the speed of the previous vehicle and finally all followers can track the speed of the leading vehicle, and all vehicles drive at fixed intervals of about 10 m.

TABLE III: Success probability of data transmission of platooning vehicle

Scenario 1		**Scenario 2**	
Vehicles	Probability	Vehicles	Probability
Follower1	0.907462	Follower1	0.910130
Follower2	0.904404	Follower2	0.906358
Follower3	0.900107	Follower3	0.901351
Follower4	0.894586	Follower4	0.895129

Fig. 5(b) shows the optimal data transmission values $\{u_i^*(k), i \in \mathcal{N}, k \in \mathcal{K}\}$ of the platooning vehicles at each time slot k. Table III tabulates the success probabilities of data transmission of each vehicle. In the whole platoon, the mean probability of successful transmission is 0.90164.

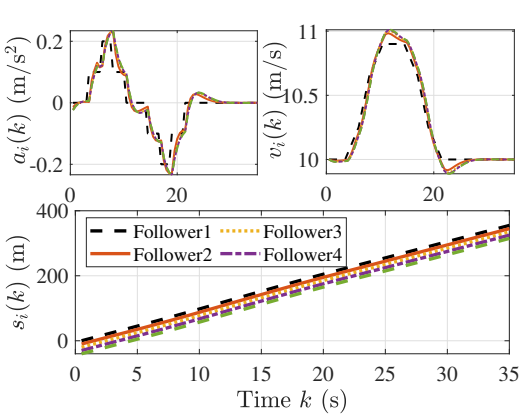

(a) The $a_i(k)$, $v_i(k)$ and $s_i(k)$ of the platooning vehicles.

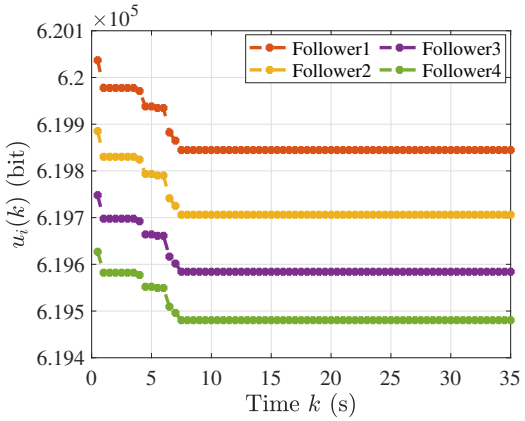

(b) The $u_i(k)$ between platooning vehicles and infrastructure.

Fig. 5: The experimental results in Scenario 1.

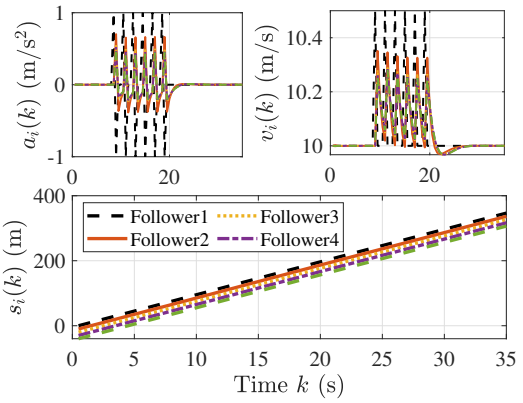

(a) The $a_i(k)$, $v_i(k)$ and $s_i(k)$ of the platooning vehicles.

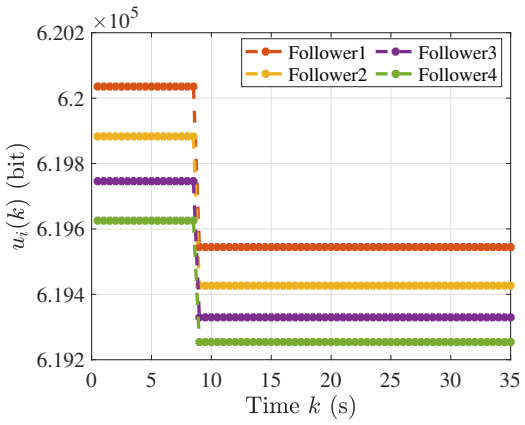

(b) The $u_i(k)$ between platooning vehicles and infrastructure.

Fig. 6: The experimental results in Scenario 2.

Moreover, the control strategy under the joint optimization method achieved the platooning objective while the resource scheduling scheme achieved the communication objective (Fig. 5(a) and 5(b)), consistent with the theoretical analysis.

In **Scenario 2**, the leading vehicle periodically accelerates and decelerates. Fig. 6(a) shows the corresponding vehicle accelerations (i.e., control inputs) $\{a_i(k), i \in \mathcal{N}, k \in \mathcal{K}\}$, speeds $\{v_i(k), i \in \mathcal{N}, k \in \mathcal{K}\}$ and longitudinal positions $\{s_i(k), i \in \mathcal{N}, k \in \mathcal{K}\}$ of each following vehicle. Fig. 6(b) shows the optimal data transmission values $\{u_i^*(k), i \in \mathcal{N}, k \in \mathcal{K}\}$ of the four following vehicles and Table III lists the success probabilities of data transmission of each vehicle. In this scenario, the mean probability of successful data transmission is 0.903242. The results of both simulation experiments showed that regardless of whether the acceleration/deceleration of the leading vehicle suddenly changed (Scenario 1) or occurred periodically (Scenario 2), the MPC controller under the joint optimization model effectively reduce the relative spacing and speed errors from the leading vehicle to its successor; meanwhile, every platoon vehicle can successfully transfer its data to the cooperative infrastructure. Interestingly, the total probability of successful data transmission is lower in Scenario 1 than in Scenario 2 (Table III), suggesting that rapid changes in the vehicle states increase the outage probability of data transmission. As confirmed in these experiments, the joint optimization model provided effective platoon control and reliable V2I communication.

E. Parameter Analysis

In this subsection, we add numerical experiments to verify further the effectiveness of the proposed joint control and communication method under different parameters, i.e., platooning vehicle number N and objective reduction rate ϵ.

1) Impact of Platooning Vehicle Number N:

First, we conduct experiments in which the number of vehicles gradually increases, i,e., from $N = 4$ to $N = 8$. We take into account the inter-vehicle average spacing error $e_N^s(k)$, average speed errors $e_N^v(k)$ to validate the control performance, and consider the average success probability of data transmission H_N to validate the V2I communication reliability. These metrics take the following forms.

$$\begin{aligned} e_N^s(k) &= \frac{\sum_{i=1}^{N}(s_{i-1}(k) - s_i(k) - d_i)}{N}, \\ e_N^v(k) &= \frac{\sum_{i=1}^{N}(v_{i-1}(k) - v_i(k))}{N}, \\ H_N &= \frac{H_{opt}}{N}. \end{aligned} \tag{53}$$

The experimental results are shown in Fig. 8. Fig. 8(a) and 8(b) plot the average inter-vehicle spacing errors $e_N^s(k)$ and average speed errors $e_N^v(k)$, respectively, as the platoon expanded from small ($N = 4$) to large ($N = 8$). Fig. 8(c) demonstrates the average data transmission success probability H_N under different platooning number N. From Fig. 8(a), we can see that the inter-vehicle average spacing error $e_N^s(k)$ of two adjacent vehicles are all within the interval [7, 13] m

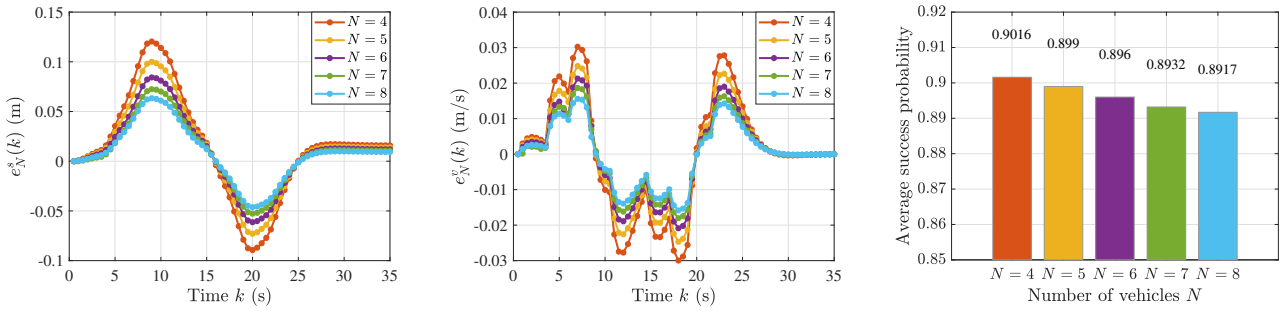

(a) The $e_N^s(k)$ under different vehicle number N. (b) The $e_N^v(k)$ under different vehicle number N. (c) The H_N under different vehicle number N.

Fig. 8: The experimental results under different vehicle number N.

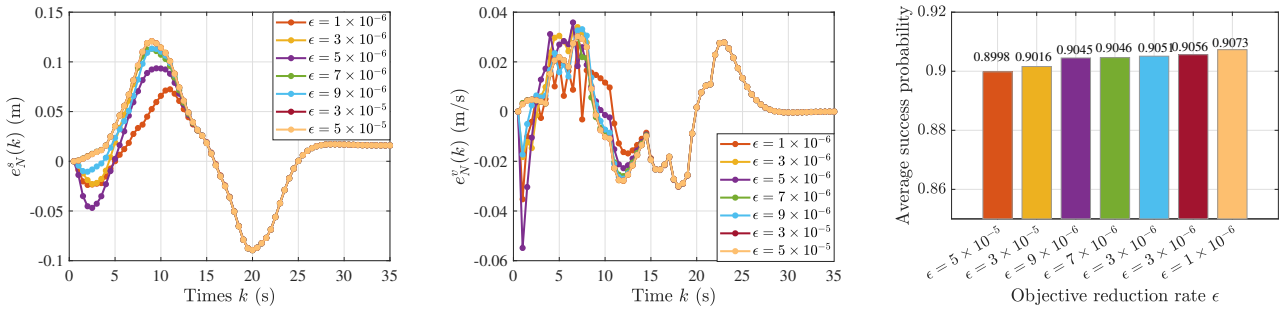

(a) The $e_N^s(k)$ under different ϵ ($N = 4$). (b) The $e_N^v(k)$ under different ϵ ($N = 4$). (c) The H_N under different ϵ ($N = 4$).

Fig. 9: The experimental results under different objective reduction rate ϵ

and finally the inter-vehicle spaces are maintained with 10 m, which implies that the platooning vehicles do not collide even with a large-scale number. In addition, 8(b) demonstrates the mean speed errors $e_N^v(k)$ under different platooning numbers. It is seen that the value of $e_N^v(k)$ can asymptotically converge to zero despite emergency acceleration and deceleration by the leading vehicle. Notably, the magnitude of the inter-vehicle average spacing error $e_N^s(k)$ and $e_N^v(k)$ decay when the vehicle number N increases, and the average success probability of data transmission H_N is decreasing. For example, the inter-vehicle spacing error is 0.0147 m, and the average data transmission success probability is 0.90164 when the platooning number $N = 4$, but the inter-vehicle spacing is 0.0084 m, and the mean data transmission success probability is 0.89631 when the platooning number $N = 8$. The main reason is that more access vehicles result in less available bandwidth being allocated to a single vehicle, and the average success probability of data transmission decreases under increasing the platooning vehicles N. It can be summarized that the proposed joint optimization method can stably realize vehicle platooning control and guarantee the reliability of data transmission with either a small-scale vehicle number (e.g., with $N = 4$) or a large-scale vehicle number (e.g., with $N = 8$).

2) Impact of Objective Reduction Rate ϵ:

Secondly, we design experiments to investigate the effect of different objective reduction rate ϵ values on the control and communication performance with the joint optimization method. The experimental results are detailed in Fig 9. In Fig. 9(a) and Fig. 9(b), we illustrate the impacts of different objective reduction rate ϵ on the average spacing $e_N^s(k)$ and average speed errors $e_N^v(k)$ of two adjacent vehicles under platooning vehicle number $N = 4$. From Fig. 9(a) and Fig. 9(b), it is seen that the total state errors achieved by the joint optimization method decline with increasing the objective reduction rate ϵ. This is because the conditions for satisfying the constraints in the model become more stringent as ϵ increases.

The total state errors in the joint optimization method declined with increasing objective reduction rate ϵ. This trend can be explained by the increasing stringency of the conditions for satisfying the model constraints as ϵ increases. The impact of ϵ on the communication reliability of the joint optimization method is displayed in Fig 9(c). Increasing ϵ will increase the average probability of successful data transmission H_N by the whole platoon. We infer that increasing the objective reduction rate ϵ decreases the lower bound $(1-\epsilon)H_{\max}(\boldsymbol{u}^*, \boldsymbol{a})$ of the communication reliability, thereby relaxing the communication constraint. Thus, the value of ϵ can be adjusted to improve the control and communication performance of our proposed joint optimization model.

F. Performance Comparison with Different Methods

We now compare the performances of the proposed joint optimization method (marked by JOM) with those of three existing optimization methods in Scenario 1. Specifically, all four cases are:

JOM(ours): This method uses a predecessor-leader following platoon vehicle tracking control protocol to design a centralised MPC controller to optimise vehicle mobility and maximise the communication reliability between the vehicles and infrastructure.

DLQR: This method uses the predecessor-following vehicle tracking control protocol to design the distributed Linear Quadratic Regulator (LQR) controllers to optimise vehicle mobility and uniformly allocates the transmission data.

DAC: This method adopts the bidirectional vehicle tracking control protocol to design the distributed acceleration controllers to optimise vehicle mobility and uniformly allocate the transmission data.

MTCR: This method maximises the communication reliability between the vehicles and infrastructure and observes the speed error and position error of the platoon vehicles.

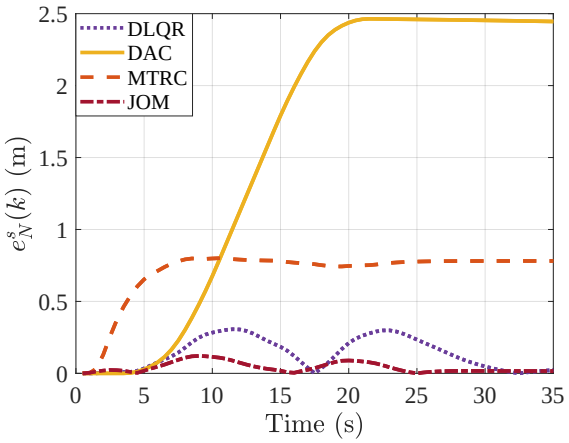

Fig. 10: The average spacing error of platoon vehicles under different method.

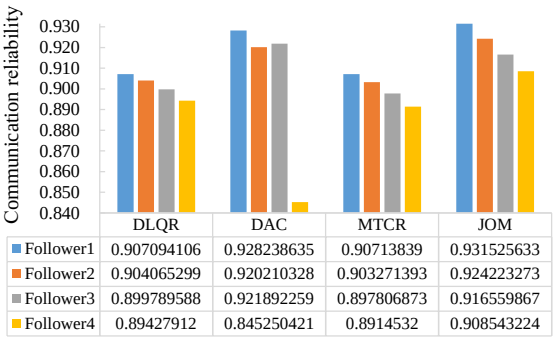

	DLQR	DAC	MTCR	JOM
Follower1	0.907094106	0.928238635	0.90713839	0.931525633
Follower2	0.904065299	0.920210328	0.903271393	0.924223273
Follower3	0.899789588	0.921892259	0.897806873	0.916559867
Follower4	0.89427912	0.845250421	0.8914532	0.908543224

Fig. 11: The communication reliability of platoon vehicle under different methods.

To better represent the differences in the optimization schemes, we show the average spacing error in Fig. 10 to assess the control performance of the platoon. In addition, we provide the V2I communication reliability objectives of a different optimization method in Fig. 11 to assess the communication performance between this platoon and the infrastructure.

Overall, our proposed bi-objective joint optimization model achieves a high probability of successful data transmission while maintaining vehicle safety with a low spacing error

in terms of platoon control. Specifically, from Fig.9, the average spacing error of this platoon is 0.040847 m, this is an improvement of 9.87% relative to method DLQR and an improvement of 65% relative to method MTRC. The average spacing error under DAC is 1.5988 m, much higher than the other three methods, which indicates that this method has the worst overall platoon control performance. By observing Fig. 11, we obtain the V2I communication performance under the four optimization methods. Obviously, under the proposed joint method, the communication reliability (success probability of data transmission) of all vehicles is 3.70457, which is higher than the other three methods. Overall, our proposed bi-objective joint optimization model achieves a high probability of successful data transmission while maintaining vehicle safety with a low spacing error in terms of platoon control.

G. Trade-off between Platoon Control and Communication Reliability

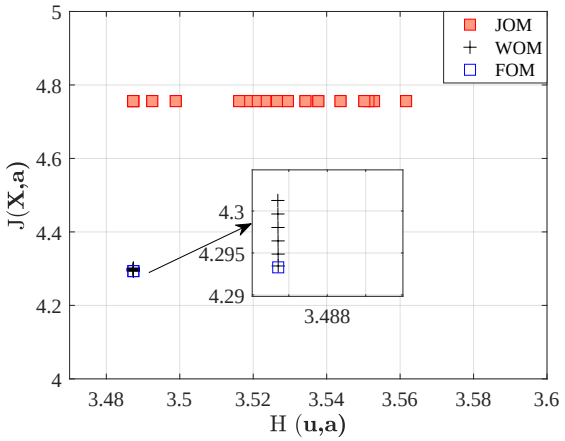

Fig. 12: The objective values under different methods.

In this paper we address the joint bi-objective optimization model M_1 based on ϵ-constraint method. To illustrate the effectiveness of this method, we compare the JOM with two other objective optimization methods. The first method is the weighted optimization method (marked by "WOM"), which optimises the weighted sum of the two objectives by introducing the weighted parameters d^+ and d^-. The objective form for WOM method is: $d^+ \times J(\boldsymbol{X}, \boldsymbol{a}) + d^- \times H(\boldsymbol{u}, \boldsymbol{a})$, where d^+ is in the range [1, 100] and d^- is in the range [1, 10^4]. The second method is the fractional optimization method (marked by "FOM"), which combines the two objectives into a single fractional form, with the optimization objective being $\frac{J(\boldsymbol{X},\boldsymbol{a})}{H(\boldsymbol{u},\boldsymbol{a})}$. For our JOM method, ϵ takes values from 10^{-6} to 10^{-4} and obtain a pareto frontier. Fig. 12 shows the two objective values under the different methods. It can be seen that the JOM method can achieve higher transmission reliability while ensuring the safety of the vehicle platoon. In addition, we are able to identify more non-dominant points. Compared to the WOM and FOM methods, our method can achieve stable travel of platoon vehicles at a distance of d_i while guaranteeing highly reliable data transmission. Specifically, our method can improve the communication reliability of the platoon system by approximately 3.6%.

VII. Conclusion

This paper investigated a communication-control joint optimization problem for a platoon-based cooperative vehicle infrastructure system. Our bi-objective optimization model aims to minimize the oscillations of the platoon while maximizing the V2I communication reliability. To this end, it combines model predictive platooning control with data transmission scheduling. We theoretically evaluated the V2I communication reliability as the overall success probability of the platoon-based data transmissions and derived a closed-form expression of optimal reliability. Using the analytical expression, we transformed the original bi-objective model into a tractable MPC problem that could be solved by an efficient iterative optimization algorithm. We also proved that the proposed algorithm always converges and verified the effectiveness of the algorithm in simulation studies. The experimental results confirmed that our proposed method can significantly improve the control stability and communication reliability of vehicle platooning.

This work is our first attempt at platoon-based communication-control joint optimization. As potential research directions, we suggest distributed control based on V2V communication technology, which is more appropriate for large-scale vehicle platoons, and control distribution based on local information of the platoon. We will explore the performance of distributed platoon control and the reliability of V2V communication. We will study the control, communication and computation ability of the joint optimization problem in the platoon-based cooperative vehicle infrastructure system.

Appendix A

Let $\Lambda = [\eta_i(k) \geq 0, i \in \mathcal{N}, k \in \mathcal{K}]^\top$, and let $\Upsilon = [\lambda_i, i \in N]^\top$ and $\lambda_i \in \mathbb{R}$ be a column vector collecting Lagrange multipliers. The Lagrange function of the sub-model is constructed as follows

$$\begin{aligned} &L(\boldsymbol{u}, \boldsymbol{a}, \Lambda, \Upsilon) = F(\boldsymbol{u}, \boldsymbol{a}) \\ &- \sum_{i=1}^{N}\sum_{k=1}^{K} \eta_i(k) u_i(k) - \sum_{i=1}^{N} \lambda_i \Big(\sum_{k=1}^{K} u_i(k) - \theta_{\text{out},i}\Big) \end{aligned} \tag{54}$$

Under the Karush–Kuhn–Tucker (KKT) conditions, the results are obtained as

$$\begin{cases} \nabla_{\boldsymbol{u}} L(\boldsymbol{u}, \boldsymbol{a}, \Lambda, \Upsilon) = \boldsymbol{0}; \\ \eta_i(k) u_i(k) = 0; \\ \sum_{k=1}^{K} u_i(k) = \theta_{\text{out},i}; \\ u_i(k) \geq 0; \\ \eta_i(k) \geq 0; \\ i \in \mathcal{N}, k \in \mathcal{K}. \end{cases} \tag{55}$$

First, the complementary relaxation condition guarantees that all optimal solutions satisfy $\eta_i(k) u_i^*(k) = 0$ for

$u_i^*(k) \in \boldsymbol{u}_i^*$. Thus, for all non-zero optimal solutions $u_i^*(k) \in \boldsymbol{u}_i^*, u_i^*(k) > 0$, we have $\eta_i(k) = 0$ and for all zero optimal solutions $u_i^*(k^{'}) \in \boldsymbol{u}_i^*, u_i^*(k^{'}) = 0$, we have $\eta_i(k^{'}) \geq 0$.

Second, the KKT system (55) ensures that every optimal solution $u_i^*(k)$ also satisfies the gradient condition

$$\begin{aligned} &\nabla_{u_i^*(k)} L\left(u_i^*(k), a_i(k), \Lambda, \Upsilon\right) = \mathbf{0} \\ \Rightarrow &\nabla_{u_i^*(k)} F(u_i^*(k), a_i(k)) - \eta_i(k) - \lambda_i = 0, i \in \mathcal{N}, k \in \mathcal{K}. \end{aligned} \tag{56}$$

Based on the above discussion of complementary relaxation conditions, the following equations hold for any optimal solution $u_i^*(\ell_1) \in \boldsymbol{u}_i^*$, $u_i^*(\ell_2) \in \boldsymbol{u}_i^*$ and $u_i^*(\ell_3) \in \boldsymbol{u}_i^*$

$$\begin{cases} \nabla_{u_i(\ell_1)} F(u_i^*(\ell_1), a_i(\ell_1)) - \eta_i(\ell_1) = 0, \ u_i^*(\ell_1) > 0; \\ \nabla_{u_i(\ell_3)} F(u_i^*(\ell_3), a_i(\ell_3)) = \eta_i(\ell_3) + \lambda_i, \ u_i^*(\ell_3) = 0, \end{cases} \tag{57}$$

where $\ell_1 \neq \ell_3$ and $\eta_i(\ell_3) + \lambda_i \geq \lambda_i$.

Therefore, the partial derivatives of the non-zero optimal solutions are all identical and cannot exceed the optimal solutions for $u_i^*(k) = 0$.

APPENDIX B

Suppose that the function $\boldsymbol{X}^\top \mathbf{Q} \boldsymbol{X} + \boldsymbol{a} \mathbf{R} \boldsymbol{a} \geq 0$, and if and only if $\boldsymbol{X} = \mathbf{0}$, $\boldsymbol{a} = \mathbf{0}$, then $\boldsymbol{X}^\top \mathbf{Q} \boldsymbol{X} + \boldsymbol{a} \mathbf{R} \boldsymbol{a} = 0$ holds. By solving the optimization problem M_2, the optimal solution of at time j is $\boldsymbol{a}_j^*$, the optimal state trajectory of the corresponding system is $\boldsymbol{X}_j^*$ and the objective value $J(\boldsymbol{X}_j^*, \boldsymbol{a}_j^*)$ is

$$J(\boldsymbol{X}_j^*, \boldsymbol{a}_j^*) = [\boldsymbol{X}_j^*]^\top \mathbf{Q} [\boldsymbol{X}_j^*] + [\boldsymbol{a}_j^*]^\top \mathbf{Q} [\boldsymbol{a}_j^*], \tag{58}$$

According to [41], the Lyapunov function $V^*(\boldsymbol{X}_j^*, \boldsymbol{a}_j^*)$ is defined as the following form

$$V_j^*(\boldsymbol{X}_j^*, \boldsymbol{a}_j^*) = J(\boldsymbol{X}_j^*, \boldsymbol{a}_j^*), \tag{59}$$

At time $j+1$, we can obtain optimal solution $\boldsymbol{a}_{j+1}^*$ and optimal state trajectory $\boldsymbol{X}_{j+1}^*$ by solving the optimization model M_2. The following equation holds

$$\begin{aligned} V_{j+1}^*(\boldsymbol{X}_{j+1}, \boldsymbol{a}_{j+1}) &= \min \ J(\boldsymbol{X}_{j+1}, \boldsymbol{a}_{j+1}) \\ &= \min \ \boldsymbol{X}_{j+1}^\top \mathbf{Q} \boldsymbol{X}_{j+1} + \boldsymbol{a}_{j+1}^\top \mathbf{R} \boldsymbol{a}_{j+1} \end{aligned}$$

For the predicted time domain k ($k = 1, \cdots, K$),

$$\begin{aligned} &V_{j+1}^*(\boldsymbol{X}_{j+1}, \boldsymbol{a}_{j+1}) \\ =&\min \ \left\{ \sum_{k=1}^{K} \boldsymbol{x}(j+k+2)^\top \mathbf{Q}_{j+1} \boldsymbol{x}(j+k+2) \right. \\ &\left. + \boldsymbol{a}(j+k+1)^\top \mathbf{R}_{j+1} \boldsymbol{a}(j+k+1) \right\} \\ =&\min \ \left\{ \sum_{k=1}^{K} \boldsymbol{x}(j+k+2)^\top \mathbf{Q}_{j+1} \boldsymbol{x}(j+k+2) \right. \\ &\left. + \boldsymbol{a}(j+k+1)^\top \mathbf{R}_{j+1} \boldsymbol{a}(j+k+1) \right\} \\ =&\min \ \left\{ \sum_{k=1}^{K} \boldsymbol{x}(j+k+1)^\top \mathbf{Q}_j \boldsymbol{x}(j+k+1) \right. \\ &+ \boldsymbol{a}(j+k)^\top \mathbf{R}_j \boldsymbol{a}(j+k) \\ &+ \boldsymbol{a}(j+K+1)^\top \mathbf{R}_{j+1} \boldsymbol{a}(j+K+1) \\ &+ \boldsymbol{x}(j+K+2)^\top \mathbf{Q}_{j+1} \boldsymbol{x}(j+K+2) \\ &\left. - \boldsymbol{x}(j+2)^\top \mathbf{Q}_j \boldsymbol{x}(j+2) + \boldsymbol{a}(j+1)^\top \mathbf{R}_j \boldsymbol{a}(j+1) \right\} \\ \leq &V_{j+1}^*(\boldsymbol{X}_{j+1}, \boldsymbol{a}_{j+1}) \\ &- \left\{ \boldsymbol{x}(j+2)^\top \mathbf{Q}_j \boldsymbol{x}(j+2) + \boldsymbol{a}(j+1)^\top \mathbf{R}_j \boldsymbol{a}(j+1) \right\} \\ &+ \min \ \left\{ \boldsymbol{a}(j+K+1)^\top \mathbf{R}_{j+1} \boldsymbol{a}(j+K+1) \right. \\ &\left. + \boldsymbol{x}(j+K+2)^\top \mathbf{Q}_{j+1} \boldsymbol{x}(j+K+2) \right\} \end{aligned}$$

For this platoon, a series of terminal equality constraints is contained in the optimization problem (M_2)

$$\boldsymbol{x}(j+K+2)^\top \mathbf{Q}_{j+1} \boldsymbol{x}(j+K+2) = \mathbf{0}. \tag{60}$$

Thus, the following equation holds with respect to the optimization objective of the terminal

$$\begin{aligned} &+ \min \ \left\{ \boldsymbol{a}(j+K+1)^\top \mathbf{R}_{j+1} \boldsymbol{a}(j+K+1) \right. \\ &\left. + \boldsymbol{x}(j+K+2)^\top \mathbf{Q}_{j+1} \boldsymbol{x}(j+K+2) \right\} = 0. \end{aligned} \tag{61}$$

Furthermore, the quadratic objective function $\sum_{k=1}^{K} \boldsymbol{x}(j+k+2)^\top \mathbf{Q}_{j+1} \boldsymbol{x}(j+k+2) + \boldsymbol{a}(j+k+1)^\top \mathbf{R}_{j+1} \boldsymbol{a}(j+k+1) \geq 0$ for all $k \in \mathcal{K}$. When $k = 1$, the following inequality holds

$$\boldsymbol{x}(j+2)^\top \mathbf{Q}_{j+1} \boldsymbol{x}(j+2) + \boldsymbol{a}(j+1)^\top \mathbf{R}_{j+1} \boldsymbol{a}(j+1) \geq 0. \tag{62}$$

Finally, we can obtain the relationship

$$\begin{aligned} &V_{j+1}^*(\boldsymbol{X}_{j+1}^*, \boldsymbol{a}_{j+1}^*) - V_j^*(\boldsymbol{X}_j^*, \boldsymbol{a}_j^*) \leq \\ &- \boldsymbol{x}(j+2)^\top \mathbf{Q}_{j+1} \boldsymbol{x}(j+2) + \boldsymbol{a}(j+1)^\top \mathbf{R}_{j+1} \boldsymbol{a}(j+1) \\ \Rightarrow &V_{j+1}^*(\boldsymbol{X}_{j+1}^*, \boldsymbol{a}_{j+1}^*) \leq V_j^*(\boldsymbol{X}_j^*, \boldsymbol{a}_j^*) \end{aligned} \tag{63}$$

APPENDIX C

We formulate the equality constraints on the system state as

$$C_m(\mathbf{U}) = \boldsymbol{x}_i(k+1) - \mathbf{A}\boldsymbol{x}_i(k) - \mathbf{B}a_{i-1}(k) - \mathbf{D}a_i(k) \quad (64)$$

for $m = 1, \ldots, 2 \times N \times (K-1)$. The equality constraints of the terminal conditions by

$$C_m(\mathbf{U}) = \boldsymbol{x}_i(K) \quad (65)$$

for $m = 2 \times N \times (K-1)+1, \ldots, 2 \times N \times K$, and the equality constraints of the total data transmission

$$C_m(\mathbf{U}) = \sum_{k=1}^{K} u_i(k) - \theta_{\text{out},i} \quad (66)$$

for $m = 2 \times N \times K + 1, \ldots, 2 \times N \times K + N$. The set of indexes related to the equality constraints can be represented by $\mathcal{M} = \{1, \ldots, 2 \times N \times K + N\}$. Similarly, the set of indexes related to inequality constraints is defined as $\mathcal{Z}$ and cardinal total number of $\mathcal{Z}$ is $5 \times N \times K + 1$. With the index z from 1 to $5 \times N \times K + 1$, the inequality constraints in joint optimization model can be rearranged as

$$C_z(\mathbf{U}) = \begin{cases} a_i(k) - a_{\min}, z = 1, \ldots, N \times K; \\ a_{\max} - a_i(k), z = N \times K + 1, \ldots, 2 \times N \times K; \\ \boldsymbol{x}_i(k) - \boldsymbol{x}_{\min}, z = 2 \times N \times K + 1, \ldots, 3 \times N \times K; \\ \boldsymbol{x}_{\max} - \boldsymbol{x}_i(k), z = 3 \times N \times K + 1, \ldots, 4 \times N \times K; \\ u_i(k), z = 4 \times N \times K + 1, \ldots, 5 \times N \times K \\ H(u_i(k), a_i(k)) \\ -(1-\epsilon)H_{\max}(u_i^*(k); a_i(k)), z = 5 \times N \times K + 1. \end{cases} \quad (67)$$

APPENDIX D

Note that $(\mathbf{U}_t,\ \boldsymbol{\lambda}_t)$ satisfy the KKT conditions, and the following gradient condition holds

$$\nabla_{\mathbf{U}} J(\mathbf{U}_t) + \mathbf{O}_t \mathbf{d}_t - \sum_{r \in \mathcal{M} \cup \mathcal{Z}} \lambda_{r,d} \nabla_{\mathbf{U}} C_r(\mathbf{U}_t) = 0. \quad (68)$$

Based on the penalty (44) and the gradient condition, we further yield

$$\begin{aligned} G'(\mathbf{U}_t, \boldsymbol{\pi}_t, \mathbf{d}_t) =& \nabla_{\mathbf{U}} J(\mathbf{U}_t)^{\mathrm{T}} \mathbf{d}_t \\ &+ \sum_{m \in \mathcal{M}} \pi_{m,t} \left| \nabla_{\mathbf{U}} C_m(\mathbf{U}_t)^{\mathrm{T}} \mathbf{d}_t \right| \\ &+ \sum_{z \in \mathcal{Z}} \pi_{z,t} \left[\max(0, -\nabla_{\mathbf{U}} C_z(\mathbf{U}_t)^{\mathrm{T}} \mathbf{d}_t) \right] \\ =& \left(\sum_{r \in \mathcal{M} \cup \mathcal{Z}} \lambda_{r,d} \nabla_{\mathbf{U}} C_r(\mathbf{U}_t) - \mathbf{O}_t \mathbf{d}_t \right)^{\mathrm{T}} \mathbf{d}_t \\ &+ \sum_{m \in \mathcal{M}} \pi_{m,t} \left| \nabla_{\mathbf{U}} C_m(\mathbf{U}_t)^{\mathrm{T}} \mathbf{d}_t \right| \\ &+ \sum_{z \in \mathcal{Z}} \pi_{z,t} \left[\max(0, -\nabla_{\mathbf{U}} C_z(\mathbf{U}_t)^{\mathrm{T}} \mathbf{d}_t) \right] \\ =& -\mathbf{d}_t^{\mathrm{T}} \mathbf{O}_t \mathbf{d}_t + \sum_{r \in \mathcal{M} \cup \mathcal{Z}} \lambda_{r,d} \nabla_{\mathbf{U}} C_r(\mathbf{U}_t)^{\mathrm{T}} \mathbf{d}_t \\ &+ \sum_{m \in \mathcal{M}} \pi_{m,t} \left| \nabla_{\mathbf{U}} C_m(\mathbf{U}_t)^{\mathrm{T}} \mathbf{d}_t \right| \\ &+ \sum_{z \in \mathcal{Z}} \pi_{z,t} \left[\max(0, -\nabla_{\mathbf{U}} C_z(\mathbf{U}_t)^{\mathrm{T}} \mathbf{d}_t) \right]. \end{aligned} \quad (69)$$

Under the constraints in (37), we have $C_m(\mathbf{U}_t) + \nabla_{\mathbf{U}} C_m(\mathbf{U}_t)^{\top} \mathbf{d}_t = 0$. Under the inequality constraints, the following complementary relaxation conditions hold

$$\begin{cases} \lambda_{z,t} \geq 0; \\ C_z(\mathbf{U}_t) + \nabla_{\mathbf{U}} C_z(\mathbf{U}_t)^{\mathrm{T}} \mathbf{d}_t \geq 0; \\ \lambda_{z,t} \left(C_z(\mathbf{U}_t) + \nabla_{\mathbf{U}} C_z(\mathbf{U}_t)^{\mathrm{T}} \mathbf{d}_t \right) = 0, \end{cases} \quad (70)$$

for all $m \in \mathcal{M}, z \in \mathcal{Z}$. In the update formula (45), $\pi_{r,t}$ and $|\lambda_{r,t}|$ satisfy $\pi_{r,t} - |\lambda_{r,t}| \geq 0$. Thus, (69) can be expressed as

$$G'(\mathbf{U}_t, \boldsymbol{\pi}_t, \mathbf{d}_t) \leq -\mathbf{d}_t^{\mathrm{T}} \mathbf{O}_t \mathbf{d}_t \leq 0, \quad (71)$$

which proves the lemma.

REFERENCES

[1] J. A. Guerrero-ibanez, S. Zeadally, and J. Contreras-Castillo, "Integration challenges of intelligent transportation systems with connected vehicle, cloud computing, and internet of things technologies," *IEEE Wireless Commun. Mag.*, vol. 22, no. 6, pp. 122–128, 2015.

[2] D. L. Fisher, M. Lohrenz, D. Moore, E. D. Nadler, and J. K. Pollard, "Humans and intelligent vehicles: The hope, the help, and the harm," *IEEE Trans. Intell. Veh.*, vol. 1, no. 1, pp. 56–67, 2016.

[3] Y. Li, W. Chen, S. Peeta, and Y. Wang, "Platoon control of connected multi-vehicle systems under v2x communications: Design and experiments," *IEEE Trans. Intell. Transport. Syst.*, vol. 21, no. 5, pp. 1891–1902, 2020.

[4] S. Tsugawa, S. Jeschke, and S. E. Shladover, "A review of truck platooning projects for energy savings," *IEEE Trans. Intell. Veh.*, vol. 1, no. 1, pp. 68–77, 2016.

[5] K. ching Chu, "Decentralized control of high-speed vehicular strings," *Transp. Sci.*, vol. 8, pp. 361–384, 1974.

[6] L. Zhang, F. Chen, X. Ma, and X. Pan, "Fuel economy in truck platooning: A literature overview and directions for future research," *J. Adv. Transport.*, vol. 2020, pp. 1–10, 2020.

[7] H. Zhou, W. Xu, J. Chen, and W. Wang, "Evolutionary v2x technologies toward the internet of vehicles: Challenges and opportunities," *Proc. IEEE.*, vol. 108, no. 2, pp. 308–323, 2020.

[8] R. Jurgen, *V2V/V2I Communications for Improved Road Safety and Efficiency*, 2012, pp. i–viii.

[9] L. Xu, L. Y. Wang, G. Yin, and H. Zhang, "Communication information structures and contents for enhanced safety of highway vehicle platoons," *IEEE Trans. Veh. Technol.*, vol. 63, no. 9, pp. 4206–4220, 2014.

[10] B. Chang, G. Zhao, L. Zhang, M. A. Imran, Z. Chen, and L. Li, "Dynamic communication qos design for real-time wireless control systems," *IEEE Sens. J.*, vol. 20, no. 6, pp. 3005–3015, 2020.

[11] C. Shao, S. Leng, Y. Zhang, A. Vinel, and M. Jonsson, "Analysis of connectivity probability in platoon-based vehicular ad hoc networks," in *2014 International Wireless Communications and Mobile Computing Conference (IWCMC)*, 2014, pp. 706–711.

[12] L. Xu, L. Y. Wang, G. Yin, and H. Zhang, "Communication information structures and contents for enhanced safety of highway vehicle platoons," *IEEE Trans. Veh. Technol.*, vol. 63, no. 9, pp. 4206–4220, 2014.

[13] A. Martínez, E. cañibano, and J. Romo, "Analysis of low cost communication technologies for v2i applications," *Appl. Sci.*, vol. 10, p. 1249, 02 2020.

[14] Q. Chen, Y. Zhou, S. Ahn, J. Xia, S. Li, and S. Li, "Robustly string stable longitudinal control for vehicle platoons under communication failures: A generalized extended state observer-based control approach," *IEEE Trans. Intell. Veh.*, pp. 1–1, 2022.

[15] H. Fuse, T. Kawabe, and M. Kawamoto, "Speed control method of electric vehicle for improving passenger ride quality," *Intelligent Control and Automation*, vol. 8, no. 1, pp. 29–43, 2016.

[16] S. E. Li, Y. Zheng, K. Li, and J. Wang, "An overview of vehicular platoon control under the four-component framework," in *2015 IEEE Intell. Veh. Symp. Proc.*, 2015, pp. 286–291.

[17] J. Zhan, Z. Ma, and L. Zhang, "Data-driven modeling and distributed predictive control of mixed vehicle platoons," *IEEE Trans. Intell. Veh.*, pp. 1–1, 2022.

[18] J. Lan and D. Zhao, "Min-max model predictive vehicle platooning with communication delay," *IEEE Trans. Veh. Technol.*, vol. 69, no. 11, pp. 12 570–12 584, 2020.

[19] Y. Yan, H. Du, D. He, and W. Li, "A pareto optimal information flow topology for control of connected autonomous vehicles," *IEEE Trans. Intell. Veh.*, pp. 1–1, 2022.

[20] F. Ma, J. Wang, S. Zhu, S. Y. Gelbal, Y. Yang, B. Aksun-Guvenc, and L. Guvenc, "Distributed control of cooperative vehicular platoon with nonideal communication condition," *IEEE Trans. Veh. Technol.*, vol. 69, no. 8, pp. 8207–8220, 2020.

[21] S. Thormann, A. Schirrer, and S. Jakubek, "Safe and efficient cooperative platooning," *IEEE Trans. Intell. Transport. Syst.*, vol. 23, no. 2, pp. 1368–1380, 2022.

[22] X. Duan, Y. Zhou, D. Tian, J. Zhou, Z. Sheng, and X. Shen, "Weighted energy-efficiency maximization for a uav-assisted multiplatoon mobile-edge computing system," *IEEE Internet Things J.*, vol. 9, no. 19, pp. 18 208–18 220, 2022.

[23] H. Zhu, Y. Zhou, X. Luo, and H. Zhou, "Joint control of power, beamwidth, and spacing for platoon-based vehicular cyber-physical systems," *IEEE Trans. Veh. Technol.*, vol. 71, no. 8, pp. 8615–8629, 2022.

[24] B. Chang, X. Yan, L. Zhang, Z. Chen, L. Li, and M. A. Imran, "Joint communication and control for mmwave/thz beam alignment in v2x networks," *IEEE Internet. Things. J.*, vol. 9, no. 13, pp. 11 203–11 213, 2022.

[25] C. Wang, Y. Dai, and J. Xia, "A cav platoon control method for isolated intersections: Guaranteed feasible multi-objective approach with priority," *Energies*, vol. 13, p. 625, 02 2020.

[26] X. T. Yang, K. Huang, Z. Zhang, Z. A. Zhang, and F. Lin, "Eco-driving system for connected automated vehicles: Multi-objective trajectory optimization," *IEEE Trans. Intell. Transport. Syst.*, vol. 22, no. 12, pp. 7837–7849, 2021.

[27] A. K. Nandi, D. Chakraborty, and W. Vaz, "Design of a comfortable optimal driving strategy for electric vehicles using multi-objective optimization," *J. Power. Sources.*, vol. 283, pp. 1–18, 2015. [Online]. Available: https://www.sciencedirect.com/science/article/pii/S0378775315003547

[28] E. Kayacan, "Multiobjective h_∞ control for string stability of cooperative adaptive cruise control systems," *IEEE Trans. Intell. Veh.*, vol. 2, no. 1, pp. 52–61, 2017.

[29] J. Zhou, D. Tian, Y. Wang, Z. Sheng, X. Duan, and V. C. Leung, "Reliability-optimal cooperative communication and computing in connected vehicle systems," *IEEE Trans. Mobile. Comput.*, vol. 19, no. 5, pp. 1216–1232, 2020.

[30] D. Niyato, E. Hossain, and P. Wang, "Optimal channel access management with qos support for cognitive vehicular networks," *IEEE Trans. Mobile. Comput.*, vol. 10, no. 4, pp. 573–591, 2011.

[31] Y. Liu, J. Zhou, D. Tian, Z. Sheng, X. Duan, G. Qu, and V. C. M. Leung, "Joint communication and computation resource scheduling of a uav-assisted mobile edge computing system for platooning vehicles," *IEEE Trans. Intell. Transport. Syst.*, pp. 1–16, 2021.

[32] A. Balador, A. Bazzi, U. Hernandez-Jayo, I. de la Iglesia, and H. Ahmadvand, "A survey on vehicular communication for cooperative truck platooning application," *Veh. Commun.*, vol. 35, p. 100460, 2022. [Online]. Available: https://www.sciencedirect.com/science/article/pii/S2214209622000079

[33] R. Oliveira, C. Montez, A. Boukerche, and M. S. Wangham, "Co-design of consensus-based approach and reliable communication protocol for vehicular platoon control," *IEEE Trans. Veh. Technol.*, vol. 70, no. 9, pp. 9510–9524, 2021.

[34] C. E. Shannon, "A mathematical theory of communication," *Bell Syst. Tech. J.*, vol. 27, no. 3, pp. 379–423, 1948.

[35] B. Sklar, "Rayleigh fading channels in mobile digital communication systems .i. characterization," *IEEE Commun. Mag.*, vol. 35, no. 7, pp. 90–100, 1997.

[36] A. Zheng and M. Morari, "Stability of model predictive control with mixed constraints," *IEEE Trans. Automat. Contr.*, vol. 40, no. 10, pp. 1818–1823, 1995.

[37] G. Mavrotas, "Effective implementation of the ϵ-constraint method in multi-objective mathematical programming problems," *Appl. Math. Comput.*, vol. 213, no. 2, pp. 455–465, 2009.

[38] M. Bartholomew-Biggs, "Constrained minimization using recursive quadratic programming," *Numerical Methods for Nonlinear Optimization*, 01 1972.

[39] M. Fukushima, Z. Q. Luo, and J. S. Pang, "A globally convergent sequential quadratic programming algorithm for mathematical programs with linear complementarity constraints," *Comput. Optim. Appl.*, vol. 10, no. 1, pp. 5–34, 1998.

[40] M. J. D. Powell, "A fast algorithm for nonlinearly constrained optimization calculations," in *Numerical Analysis*, G. A. Watson, Ed. Berlin, Heidelberg: Springer Berlin Heidelberg, 1978, pp. 144–157.

[41] Y. Zheng, S. E. Li, K. Li, F. Borrelli, and J. K. Hedrick, "Distributed model predictive control for heterogeneous vehicle platoons under unidirectional topologies," *IEEE Trans. Contr. Syst. Technol.*, vol. 25, no. 3, pp. 899–910, 2017.

Peiyu Zhang received her M.S. degree in mathematics from Heibei University, Baoding, China, in 2020. She is currently pursuing the Ph.D. degree with the School of Transportation Science and Engineering, Beihang University, Beijing, China. Her main research interests include vehicle platoon control, intelligent transportation systems and robust optimization.

Daxin Tian received his Ph.D degree in computer application technology from Jilin University, Changchun, China, in 2007. He is currently a professor with the School of Transportation Science and Engineering, Beihang University, Beijing, China. His research is focused on intelligent transportation systems, autonomous connected vehicles, swarm intelligent and mobile computing. He was awarded the Changjiang Scholars Program (Young Scholar) of Ministry of Education of China in 2017, the National Science Fund for Distinguished Young Scholars in 2018, and the Distinguished Young Investigator of China Frontiers of Engineering in 2018. He is also a sensor member of the IEEE ans served as the Technical Program Committee member/Chair/Co-Chair for several international conferences including EAI 2018, ICTIS 2019, IEEE ICUS 2019, IEEE HMWC 2020, GRAPH-HOC 2020, etc.

Jianshan Zhou received the B.Sc., M.Sc., and Ph.D. degrees in traffic information engineering and control from Beihang University, Beijing, China, in 2013, 2016, and 2020, respectively. He is an associate professor with the school of transportation science and engineering at Beihang University. From 2017 to 2018, he was a Visiting Research Fellow with the School of Informatics and Engineering, University of Sussex, Brighton, U.K. He was a Postdoctoral Research Fellow supported by the Zhuoyue Program of Beihang University and the National Postdoctoral Program for Innovative Talents from 2020 to 2022. He is or was the Technical Program Session Chair with the IEEE EDGE 2020, the IEEE ICUS 2022, the ICAUS 2022, the TPC member with the IEEE VTC2021-Fall track, and the Youth Editorial Board Member of the Unmanned Systems Technology. He is the author or co-author of more than 30 international scientific publications. His research interests include the modeling and optimization of vehicular communication networks and air–ground cooperative networks, the analysis and control of connected autonomous vehicles, and intelligent transportation systems. He was the recipient of the First Prize in the Science and Technology Award from the China Intelligent Transportation Systems Association in 2017, the First Prize in the Innovation and Development Award from the China Association of Productivity Promotion Centers in 2020, the Second Prize in the Beijing Science and Technology Progress Award in 2022, the National Scholarships in 2017 and 2019, the Outstanding Top-Ten Ph.D. Candidate Prize from Beihang University in 2018, the Outstanding China-SAE Doctoral Dissertation Award in 2020, and the Excellent Doctoral Dissertation Award from Beihang University in 2021.

Xuting Duan received the Ph.D degree in Traffic Information Engineering and Control from Beihang University, Beijing, China. He is currently an assistant professor with the School of Transportation Science and Engineering, Beihang University. His current research interests include vehicular ad hoc networks, cooperative vehicle infrastructure system and internet of vehicles.

Zhengguo Sheng received the B.Sc. degree from the University of Electronic Science and Technology of China, Chengdu, China, in 2006, and the M.S. and Ph.D. degrees from Imperial College London, London, U.K., in 2007 and 2011, respectively. He is currently a Senior Lecturer with the University of Sussex, Brighton, U.K. Previously, he was with UBC, Vancouver, BC, Canada, as a Research Associate, and with Orange Labs, Santa Monica, CA, USA, as a Senior Researcher. He has more than 100 publications. His research interests include the IoT, vehicular communications, and cloud/edge computing.

Dezong Zhao received the B.Eng. and M.S. degrees from Shandong University, Jinan, China, in 2003 and 2006, respectively, and the Ph.D. degree from Tsinghua University, Beijing, China, in 2010, all in Control Science and Engineering. He is a Senior Lecturer in Autonomous Systems with the School of Engineering, University of Glasgow, U.K. Dr Zhao's research interests include connected and autonomous vehicles, machine learning and control engineering. His work has been recognised by being awarded an EPSRC Innovation Fellowship and a Royal Society-Newton Advanced Fellowship in 2018 and 2020, respectively.

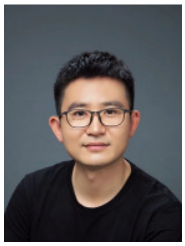

Dongpu Cao received the Ph.D. degree from Concordia University, Canada, in 2008. He is the Canada Research Chair in Driver Cognition and Automated Driving, and currently an Associate Professor and Director of Waterloo Cognitive Autonomous Driving (CogDrive) Lab at University of Waterloo, Canada. His current research focuses on driver cognition, automated driving and cognitive autonomous driving. He has contributed more than 200 papers and 3 books. He received the SAE Arch T. Colwell Merit Award in 2012, IEEE VTS 2020 Best Vehicular Electronics Paper Award and three Best Paper Awards from the ASME and IEEE conferences. Prof. Cao serves as Deputy Editor-in-Chief for IET INTELLIGENT TRANSPORT SYSTEMS JOURNAL, and an Associate Editor for IEEE Transactions on Vehicular Technology, IEEE Transactions on intelligent transportation systems, IEEE/ASME Transactions on Mechatronics, IEEE Transactions on Industrial Electronics, IEEE/CAA JOURNAL OF AUTOMATICA SINICA, IEEE Transactions on computational social systems, and ASME Journal of Dynamic Systems, Measurement and Control. He was a Guest Editor for Vehicle System Dynamics, IEEE TRANSACTIONS ON SMC: SYSTEMS and IEEE INTERNET OF THINGS JOURNAL. He serves on the SAE Vehicle Dynamics Standards Committee and acts as the Co-Chair of IEEE ITSS Technical Committee on Cooperative Driving.